universität wien

MASTERARBEIT / MASTER'S THESIS

Titel der Masterarbeit / Title of the Master's Thesis

„ Synthesis of 1,4-Dicarbonyl via [3,3]-sulfonium rearrangement: Computational Investigation and Application to Heterocycle Formation “

verfasst von / submitted by

Laurin Pollesböck, BSc

angestrebter akademischer Grad / in partial fulfilment of the requirements for the degree of

Master of Science (MSc)

Wien, 2022 / Vienna 2022

Studienkennzahl lt. Studienblatt / degree programme code as it appears on the student record sheet:	UA 066 862
Studienrichtung lt. Studienblatt / degree programme as it appears on the student record sheet:	Masterstudium Chemie
Betreut von / Supervisor:	Univ.-Prof. Dr. Nuno Maulide
Mitbetreut von / Co-Supervisor:	Dr. Boris Maryasin

Zusammenfassung

Die Carbonyl Gruppe wird weitgehend als eine der vielfältigsten und synthetisch wertvollsten funktionellen Gruppen der organischen Chemie betrachtet. Während 1,3- und 1,5-Dicarbonyle durch ihre natürliche Polarität einfache Synthesewege bieten, müssen für 1,4-Dicarbonylsynthese aufwendigere Strategien verfolgt werden. Die Arbeitsgruppe von Prof. Nuno Maulide hat vor einiger Zeit eine neue Methode für die Synthese dieses anspruchsvollen Kohlenstoffgerüsts entwickelt. Hierbei werden Ynamide und Vinylsulfoxide verwendet, wobei der Hauptschritt eine ladungsbeschleunigte sigmatrope Umlagerung darstellt.

In dieser Arbeit wurde der Mechanismus der zuvor beschriebenen Synthese mit quantenmechanischen Rechnungen im Detail untersucht, um bisher ungeklärte Zusammenhänge aufzudecken. Vor allem die Diastereoselektivität stand im Fokus der Arbeit, da diese von bisher ungeklärten Faktoren stark beeinflusst wird. Außerdem wurden die hergestellten 1,4-Dicarbonylverbindungen auf ihre Reaktivität mit Nukleophilen untersucht, um wertvolle y-substituierte Lactame und Lactone herzustellen.

Abstract

The carbonyl group is arguably the most versatile and synthetically valuable functional group in organic chemistry. While 1,3- and 1,5-dicarbonyls are easily accessible due to the natural polarity of the carbonyl group, more elaborate approaches must be applied to achieve 1,4-dicarbonyl compounds. The research group of Prof. Nuno Maulide has recently developed a novel methodology for the synthesis of this challenging scaffold. Utilising ynamides and vinylsulfoxides, the reaction relies on a charge accelerated sigmatropic rearrangement as the key step.

In this work, the mechanism of the aforementioned process was studied in-depth computationally to shed light on undisclosed aspects of the reaction mechanism. A major focus of the computational work was to determine factors influencing changes in diastereoselectivity. Additionally, the 1,4-dicarbonyl compounds synthesised via this method were further investigated for follow-up transformations towards highly sought-after γ-lactone and lactam scaffolds.

Acknowledgements

First, I would like to thank my supervisor Univ.-Prof. Nuno Maulide for the opportunity to be part of his ambitious project to advance the understanding of organic chemistry. His engaging lectures and challenging exams inspired a passion for solving intricate organic chemistry puzzles, which is regularly embraced in his group's Denksport sessions and kitchen discussions.

I would like to thank Dr. Boris Maryasin for giving me a new and fascinating tool to dive even deeper into challenging riddles of organic chemistry, teaching me most of what I know now about computational chemistry. No matter what kind of problems I encountered during my computational investigations, Boris has been there before and knew the solution.

Thank you to Univ.-Prof. Leticia González and her whole research group for the warm welcome I received as a beginner to computational chemistry and the opportunity to learn about a lot of research topics outside of my comfort zone.

A big thank you goes out to Dr. Margaux Riomet, who not only showed me a lot of practical skills in the lab, but also encouraged me with everlasting optimism when the going was though. Thank you Dr. Immo Klose and Dr. Nicolas Simonian for always being there for my countless questions about the challenging project I was working on. Obrigado to Carlos Goncalves and Ricardo Meyrelles, since I could not have survived my internship without a Portuguese colleague close-by to cheer me up with not too politically correct humour. Also I would like to thank Stefanie Rukavina, who started her internship together with me and always pushed me to fill all the official forms in time.

I would like to thank the whole Maulide group for the amazing company, for the easy-going lab, office, and kitchen atmosphere, inspiring discussions, and the countless evenings spent together: Haoqi Zhang, Bogdan Brutiu, amazing and powerful Ing. Martina Drescher, Dr. Daniel Kaiser, Miran Lemmerer, Dr. David Just, Milos Vavrik, Mag. Patricia Emberger, Iakovos Saridakis, Manuel Schupp, Philipp Spieß, Christian Knittl-Frank, Sergio Armentia Metheu, Dr. Thomas Leischner, Dr. Phillip Grant, Dr. Minghao Feng, Roberto Tinelli, Yi Xiao, Dr. Saad Shaaban, Vincent Porte, Ass.-Prof. Dr. Harry Martin, Ing. Elena Macoratti, Dr. Anthony

Fernandes-Goodall, Irmgard Tiefenbrunner, Dr. Ana Sirvent Verdú, Magdalena Mishevska, Omar Abdo, Dr. Giovanni Di Mauro

A big thanks goes to my family and friends for reminding me that there is a world outside the lab and office. Especially I thank Kreativsport Verein for fulfilling the need for sport and amazing company at the same time. Finally, I would like to thank my friends Thomas, Severin, Konstantin, and Ines for threatening to donate money to the FPÖ if I fail to write enough pages of my thesis each week. I also like to thank the FPÖ for being despicable enough to serve as a very motivating threat.

List of Abbreviations

AcOH	Acetic acid
B3LYP	Becke, 3-parameter, Lee-Yang-Parr density functional
BOA	Born Oppenheimer approximation
CAN	ceric ammonium nitrate $(NH_4)_2Ce(NO_3)_6$
CC	coupled cluster
χ	one-electron wave function
CPCM	conductor-like polarisable continuum model
CREST	conformer-rotamer ensemble sampling tool
d.r.	diastereomeric ratio
DFT	density functional theory
DLPNO-CCSD(T)	domain based local pair natural orbital coupled cluster
DTBP	di-*tert*-butyl peroxide
E	electrophile
E	energy
eq. or equiv.	equivalents
ESI	electron spray ionisation
EWG	electron withdrawing group
G	Gibbs energy
GFN-FF	geometr, frequency and non-covalent interaction force field method
GTO	Gaussian type orbital
H	Hamilton operator
HF	Hartree-Fock
HMPA	hexamethylphosphoramide
KHMDS	potassium bis(trimethylsilyl)amide
KS	Kohn-Sham model
LCMS	liquid chromatography mass spectrometry
LDA	lithium diisopropylamide
LiHMDS	lithium bis(trimethylsilyl)amide

N	number of electrons
NEB	nudged elastic band
NHC	N-heterocyclic carbene
NMR	nuclear magnetic resonance spectroscopy
Nu	nucleophile
PCM	polarisable continuum model
PES	potential energy surface
Φ	approximated wave function of a system
PMP	para-methoxy-phenyl
Ψ	exact wave function of a system
p-Tol	para-tolyl
quant.	quantitative yield
R	nuclear coordinates
r	electronic coordinates
r.t.	room temperature
SCRF	self-consistent reaction field
SM	starting material
SMD	solvent model based on electron density
STO	Slater type orbital
Tf_2N^-	bis(trifluoromethane)sulfonimide
Tf_2NH	bis(trifluoromethane)sulfonimidic acid
TFA	trifluoroacetic acid
THF	tetrahydrofuran
TISE	time independent Schrödinger equation
TMS	trimethylsilyl
Tol-spec	para-tolyl spectator ligand
TS	transition state
$\vec{x}$	electron coordinate vector
xTB	extended tight-binding model

Table of contents

1. Introduction

1.1 Organic Chemistry

1.1.1 Dicarbonyls: Synthesis

The carbonyl functionality is arguably one of the most versatile and abundant functional group in organic compounds. In particular, compounds with more than one carbonyl function are highly valuable building blocks.[1] To differentiate between different dicarbonyl scaffolds (e.g., 1,3; 1,4; or 1,5) numbers are used, indicating the relative distance in carbon atoms between them (Figure 1). Due to their high importance, several strategies for their preparation have been developed.

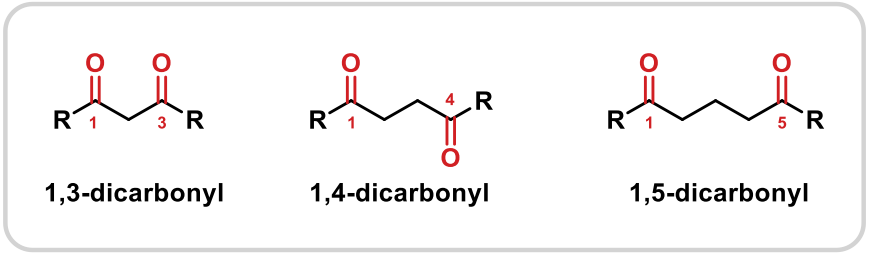

Figure 1: Different dicarbonyl functionalities and the corresponding nomenclature

One of the typical methods to access 1,3-dicarbonyls is **Claisen condensation** of an enolate (derived from an ester or ketone) and an ester, following the natural polarity of the carbonyl functionality (Figure 2, **A**). The reaction proceeds under of a base treatment.[2,3]

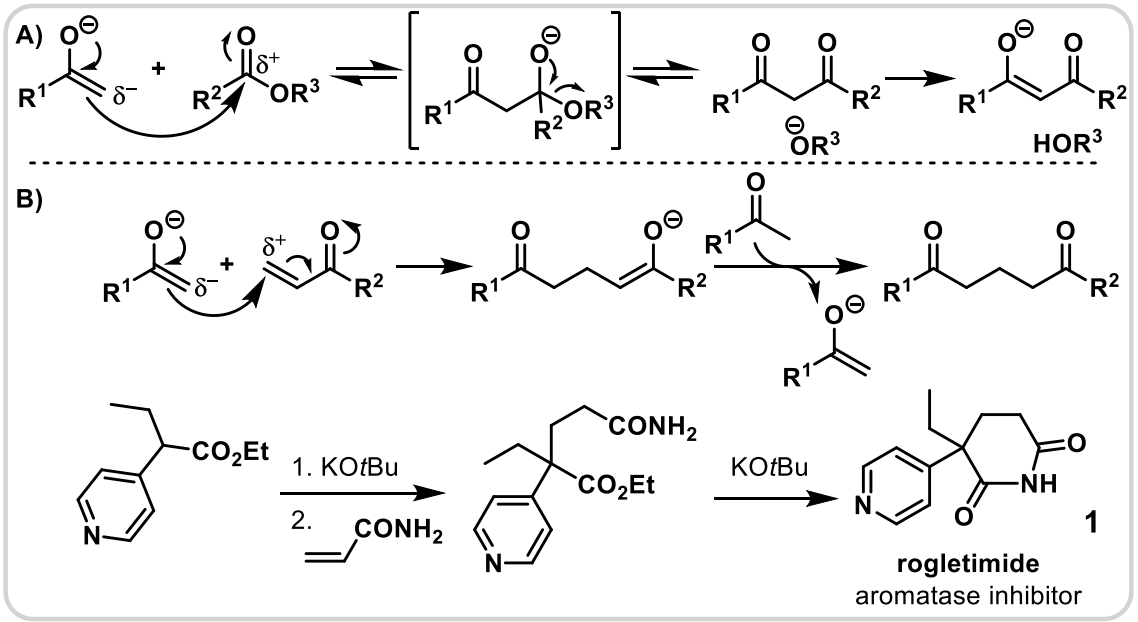

Figure 2: A) Synthesis of 1,3-dicarbonyls via Claisen condensation. B) Access of 1,5-dicarbonyls via Michael-addition of enolate with Michael acceptor and its application in the synthesis of rogletimide[4]

Michael-addition is a frequently used method for obtaining 1,5-dicarbonyl compounds in a straightforward way, also relying on enolate chemistry (Figure 2, **B**). In this case, an enolate addition to α,β-unsaturated carbonyls (known as Michael-acceptors) takes place in the positively polarised β-position. In contrast to Claisen condensations, it is possible to use a catalytic amount of base, since the formed enolate is not stabilised by a second carbonyl and can therefore act as a base. [3,5] A textbook example for a total synthesis application of Michael-addition is the synthesis of rogletimide (**1**).[4]

While the synthesis of 1,3- and 1,5-dicarbonyls can follow the intrinsic polarity of the carbonyl functionality, which facilitates synthesis, **1,4-dicarbonyl** synthesis is more challenging. At the same time, its ubiquity in natural compounds and drugs as well as the versatility as a heterocycle precursor make it a much appealing target functionality for organic synthesis (Figure 3). [6–8]

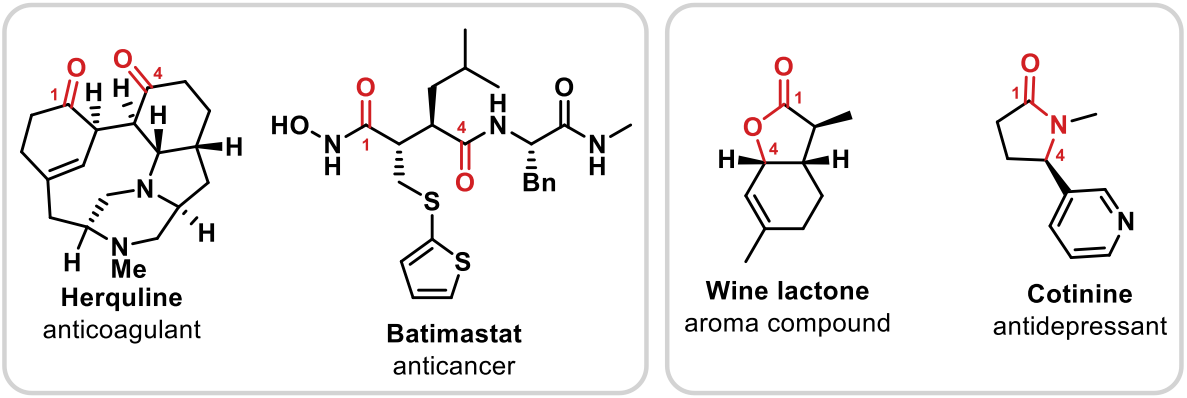

Figure 3: Selected examples of natural products and drugs containing 1,4-dicarbonyl scaffolds (left) and potential cyclic derivatives (right)

Modern synthetic methods rely on oxidative enolate coupling (Figure 4, **A-C**) or Umpolung strategies (Figure 4, **D-E**). First reports of oxidative enolate coupling go back to 1935, but synthetically relevant procedures were only developed in the 1970s.[9] The field was later greatly expanded by Baran et al.,[10] enabling moderately diastereoselective synthesis (Figure 4, **B**). MacMillan and co-workers have also reported an enantioselective organo-catalysed synthesis of 1,4-dicarbonyls via the reaction of silyl enolates with aldehydes (Figure 4, **C**). [11]

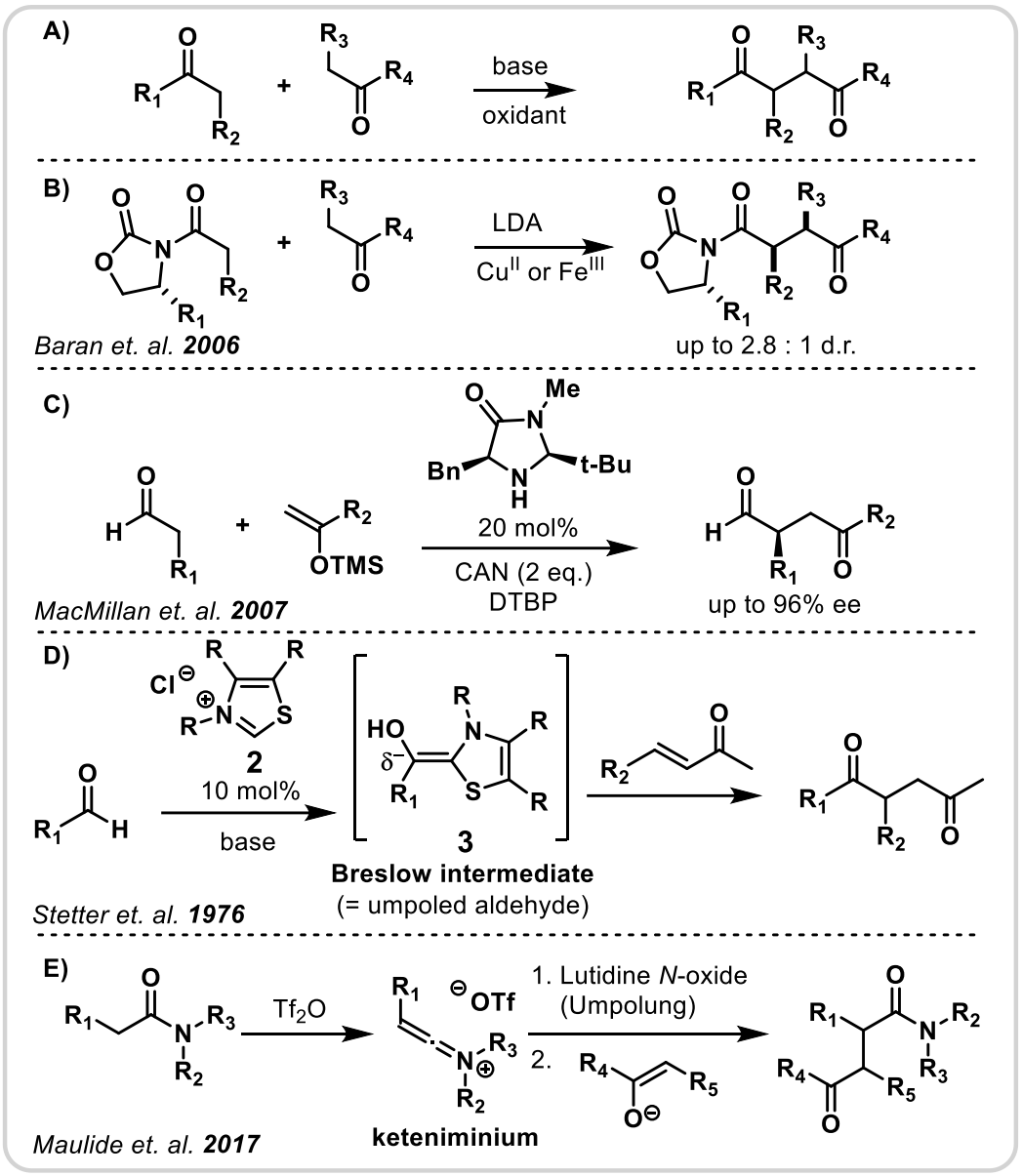

Figure 4: Previously reported oxidative enolate coupling (A-C) and Umpolung (D,E) strategies to access 1,4-dicarbonyl scaffolds

Umpolung (polarity inversion) is a term that refers to the change of polarity for a functional group. One of the most prominent examples is the Stetter reaction (Figure 4, **D**). The reaction typically utilises *N*-heterocyclic carbene (NHC) catalysts (**2**) to achieve the Umpolung of aldehydes.[12] The resulting acyl anion synthon, called Breslow intermediate (**3**), can then undergo nucleophilic attack to a Michael-acceptor to afford 1,4-dicarbonyl derivatives.[13] Modern variants of the Stetter reaction can utilise chiral NHC catalysts to achieve asymmetric transformations.[14] Maulide et. al. developed a 1,4-dicarbonyl synthesis by Umpolung of keteniminium ions formed by amide activation (Figure 4, **E**).[15]

1.1.2 The Reactivity of Ynamides

The alkyne motif, omnipresent in organic chemistry, represents a versatile building block due to its different modes of reactivity. However, for internal alkynes, low polarisation implies that regioselectivity issues can arise. When substituted with a heteroatom, such as nitrogen (as in so-called **ynamines,** Figure 5, **A**, left), the triple bond becomes polarised, leading to a higher reactivity, while at the same time differentiating the two sp-hybridised carbon atoms. As a result, ynamines are appealing reaction partners in organic chemistry, yet their lack of stability and propensity towards hydrolysis limited their development.

To overcome the stability issues, the nitrogen high electron density can be modulated with the introduction of electron-withdrawing groups. At first inductively effective moieties (e.g., CF_3) or aromatic groups were employed (Figure 5, **A**, right). Later, carbonyl groups became the dominant stabilising moieties. These *N*-alkynyl amides, known as **ynamides** (Figure 5, **B**) are easily handled and display a great balance between reactivity and stability.

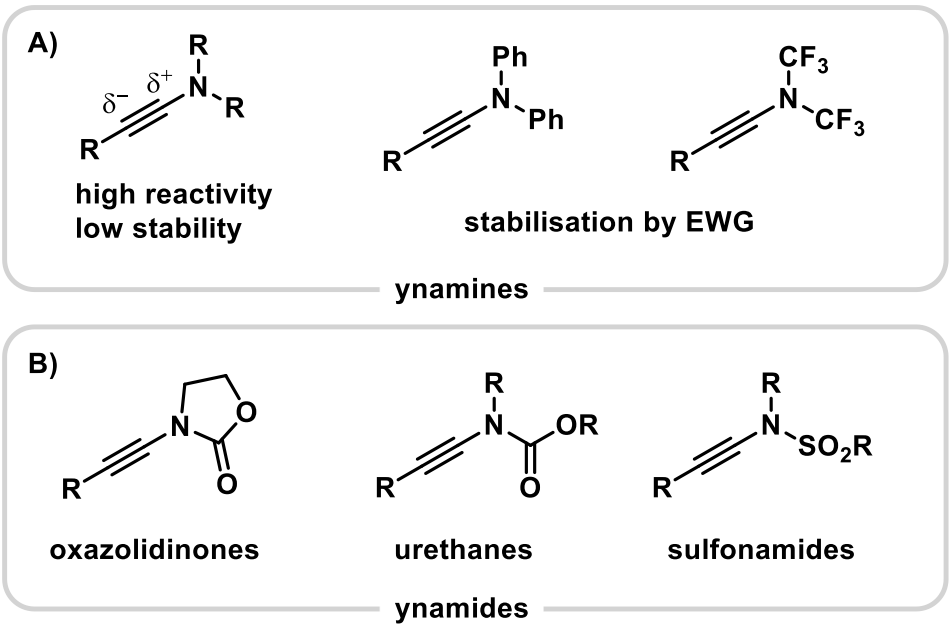

Figure 5: Examples for synthetically valuable ynamines and ynamides.

Several approaches have been developed for **ynamide synthesis** ranging from isomerisation of propargylamides through to elimination reactions of α-halo enamides (Figure 6, **A**) to more modern synthesis methods relying on direct alkynylation of *N*-nucleophiles (Figure 6, **B-D**).[16–

[18] Both the isomerisation and elimination approaches are restricted to a very limited number of substrates. Amination of alkynyl hypervalent iodonium salts (Figure 6, **B**) was the most popular method until the development of copper mediated alkynylation.

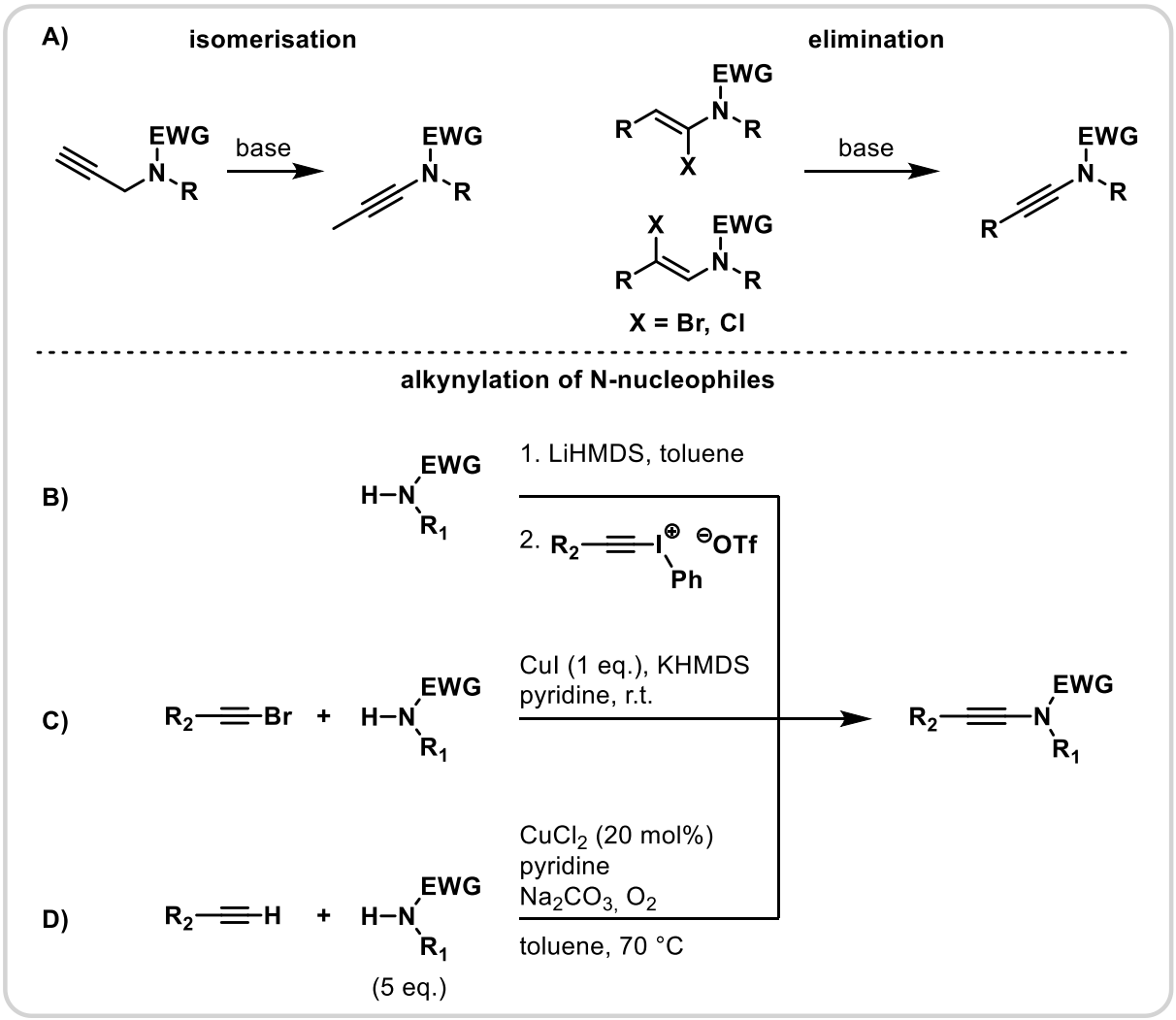

Figure 6: Ynamide synthesis, historical (A, B) and modern (C, D) approaches

Copper-promoted synthesis of ynamides from alkynyl bromides allows access to a wide range of products (Figure 6, **C**).[18,19] The copper-catalysed **oxidative alkynylation** of carbamates and sulfonamides with terminal alkynes, developed by Stahl and co-workers (Figure 6, **D**), [20] provides an elegant method for large scale ynamide synthesis with excellent yields. Drawbacks include the necessity of five equivalents of *N*-nucleophile to prevent dimerisation through Glaser-Hay coupling.[21,22]

Ynamide reactivity is driven by the electron-donating properties of the nitrogen, which strongly polarises the triple bond. This polarised bond can react regioselectively with both electrophiles and nucleophiles (Figure 7). A common way to increase the reactivity towards nucleophiles is by treatment with a Brønsted acid, forming the highly reactive keteniminium ion (**4**).

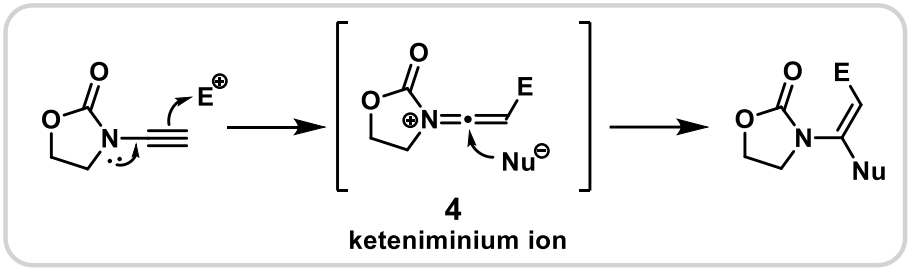

Figure 7: Reactivity of ynamides with nucleophiles and electrophiles

Important **transformations using keteniminium** ions include cycloadditions (Figure 8, **A**), [23–25] regioselective Friedel-Crafts reaction of heteroaromatic systems (Figure 8, **B**)[26] and nucleophilic additions of allylic or propargylic alcohols, followed by [3,3]-sigmatropic rearrangement (Figure 8, **C**).[27,28]

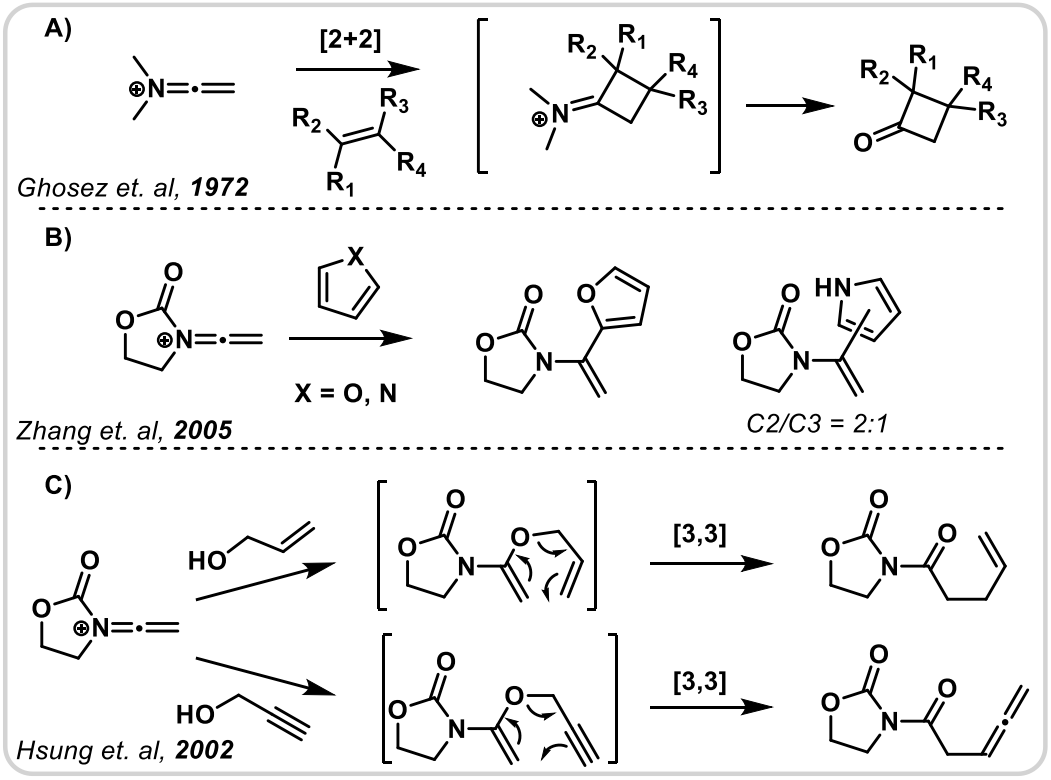

Figure 8: Selected examples of important keteniminium transformations

First reported by L. Claisen in 1912[29], **[3,3]-sigmatropic rearrangements** are a powerful and versatile tool for carbon-carbon bond formation. Modifications of the Claisen rearrangement have later been developed, most notably by Ireland, Johnson and Eschenmoser, using different substrate classes[30]. This family of transformations allows, thanks to structurally rigid transition state geometries, for very good diastereoselectivity during the formation of new chiral centres.

Generally, Claisen rearrangements are considered to proceed via a **chair**-like transition state (Figure 9, **A**). However, some examples show inverse selectivity, indicating the intermediacy of a **boat** conformation (Figure 9, **B**).[31] Several **experimental**[32] and **computational**[33,34] studies have been conducted to clarify the nature of [3,3]-transition states. However, a consistent approach to predict whether a given reaction will involve a chair or boat conformation remains elusive.

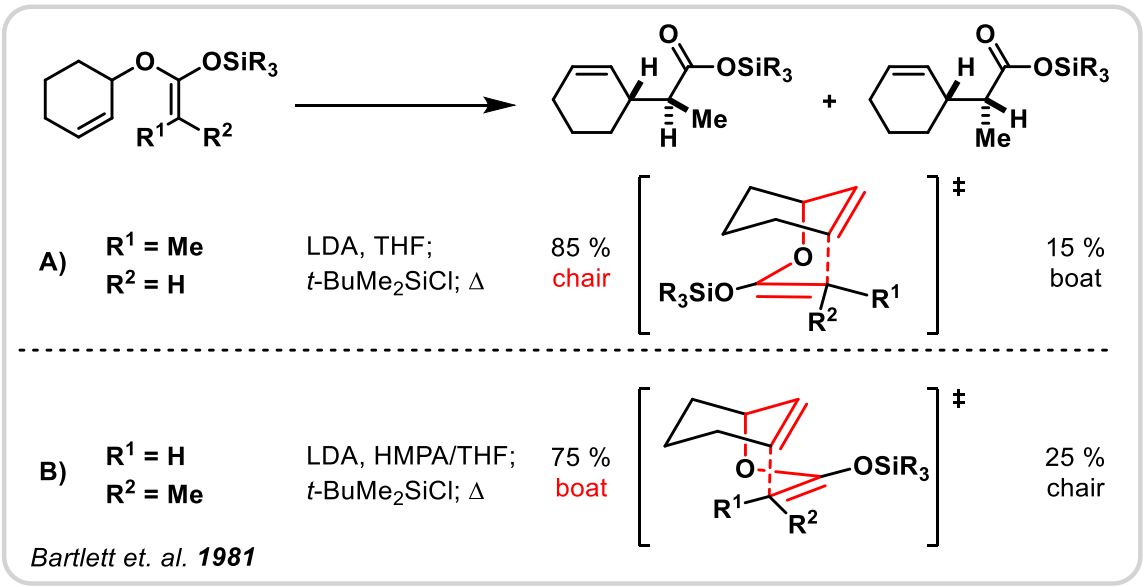

Figure 9: Example of chair and boat transition state preference through [3,3]-Claisen rearrangement

Considering the reactivity of keteniminium ions with allylic alcohols, Maulide and co-workers designed a powerful transformation employing **vinyl sulfoxides** (**5**) as nucleophiles. The addition product (**enolonium, 6**) can undergo a charge-accelerated [3,3]-sigmatropic rearrangement (Figure 10).[35–37] Due to the intrinsic chirality of sulfoxides, excellent chirality transfer from sulfur to carbon could be achieved when using optically pure vinylsulfoxides.[38,39]

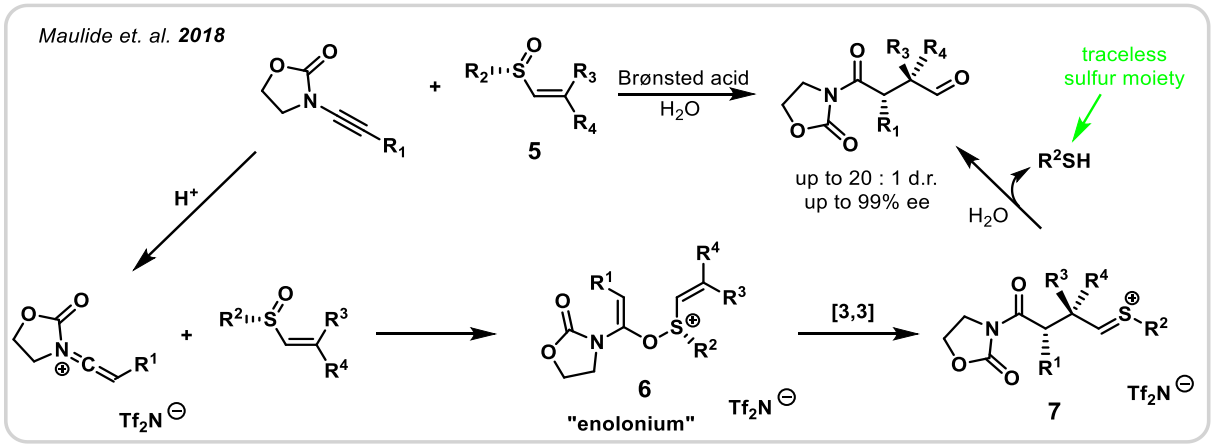

Figure 10: Reaction overview and key steps of the mechanism for 1,4-dicarbonyl synthesis developed by Maulide and co-workers

Upon hydrolysis, the [3,3]-sulfonium rearrangement products (**7**) of vinylsulfoxides yield **1,4-dicarbonyl** scaffolds with excellent enantiomeric excess and very good d.r. for a wide range of substrates. The sulfur moiety, origin of the chiral information, is hereby removed from the final product (Figure 10), in contrast to other popular auxiliaries. **R^2** is also called the **spectator ligand**.

This novel approach allows for stereodivergent access to all 4 possible stereoisomers of a given 1,4-dicarbonyl array (Figure 11). The product stereochemistry is dictated by the vinylsulfoxide only. Its double bond geometry dictates the relative configuration and the sulfoxide's chirality is transferred as the absolute configuration. While the transformation tolerates different substitution patterns for most *E*-sulfoxides, the diastereoselectivity with *Z*-sulfoxides is more substrate dependent. The correlation factors for this cannot be determined intuitively, which is why computational investigation of the problem was conducted.

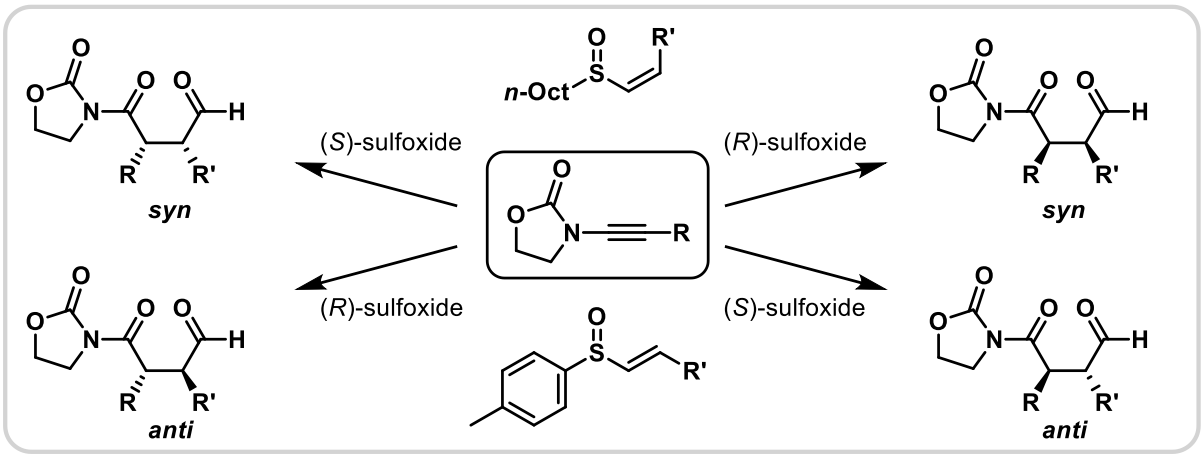

Figure 11: Stereodivergent novel 1,4-dicarbonyl synthesis pathway allows access to all 4 possible isomers.

1.2 Computational Chemistry

1.2.1 General Concepts of Theoretical Chemistry

To obtain the full picture of an organic reaction, it is often crucial to investigate not only by experiment, but by consulting quantum chemical calculations to clarify the underlying reaction mechanism. While a comparison of a reaction's energy minima can predict thermodynamic preferences, the reaction kinetics are correlated to the energies of the corresponding transition states. The energy of an investigated system can be calculated by solving the time-independent **Schrödinger equation** (TISE) (1). [40–42]

$$\mathbf{H}(r,R)\Psi(r,R) = E\,\Psi(r,R) \tag{1}$$

While the TISE can be solved for two particle systems, approximations must be applied for larger systems. Due to the substantial mass and speed difference between electrons and nuclei, it is in many cases valid to neglect the movement of the nuclei, which is called **Born-Oppenheimer approximation** (BOA). The electronic wave functions can then provide a potential energy surface (PES) as a function of the nuclear positions, which in turn yields valuable information about involved reaction mechanisms. [40–42]

The kinetic energy of the investigated electrons is highly dependent on the dynamics of other electrons in the system. Many-electron models are very complicated, leading to another major approximation by averaging the electronic interactions: the **Hartree-Fock** (HF) theory.[40] In HF theory, the *N*-electron wave function Ψ_0 is approximated by introducing a Slater determinant Φ_{SD}, which consists of N independent one-electron functions χ_i (x_i) called "orbitals." (2)[43]

$$\Psi_0 \approx \Phi_{SD} = \frac{1}{\sqrt{N!}} \det\{\chi_1(\vec{x}_1)\ \chi_2(\vec{x}_2) \ldots \chi_N(\vec{x}_N)\} \tag{2}$$

To construct the wave function for solving the Schrödinger equation, a set of mathematical functions is used, called a **basis set**. Each molecular orbital is hereby formulated as a linear combination of the basis functions of the individual atoms, which are defined in the chosen basis set. While Slater-type orbitals (STOs) are better in describing the physical behaviour of

electrons, the integral evaluation is easier with Gaussian-type orbitals (GTOs) than with STOs.[44]

Depending on the investigated problem, computational chemists can rely on an immense array of different basis sets of varying size. While bigger basis sets tend to give more accurate results, the computational cost is also increased significantly. In this project, basis sets of the def2-series, developed in Karlsruhe by Ahlrichs and co-workers,[45] have been used due to their reliability in combination with the methods applied in this project.

With increasingly large basis sets, and even in the case of the complete basis set limit CBS (extrapolated estimate), remains the difference between the HF energy and exact energy (E_0).[40] This gap is called the **electron correlation energy** (E_C). Even though the HF method yields the best possible wave function that can be described with one determinant, for the accurate description of physical and chemical properties, more determinants, including excited configurations, can be required.

$$E_0 = E_{HF(CBS)} + E_C \tag{3}$$

There are different approaches of including electron correlation into quantum chemical calculations with one of the most prominent being **coupled cluster** (CC). In the notation of this methods, letters are included, indicating which kinds of excitation are considered. Considering computational feasibility and increase in accuracy, CC methods including single (S) and double (D) excitations are the most common. The CCSD method neglects the triple and higher-order excitations, which is why hybrid methods were introduced, which include the triples energy using perturbation theory and add it to the CCSD result.[46] One of these methods is called CCSD(T) and is widely recognised as the "gold-standard" of computational organic chemistry.[47]

A method that can speed up CC calculations at very minor loss of accuracy is the **domain-based pair natural orbital coupled cluster** (DLPNO-CC) theory.[47,48] In contrast to other CC methods its computation time scales almost linearly with increasing system size, while at the same time keeping the loss in correlation energy very small (< 0.05 % on average). The major downside

of this method is, it can only be used for energy calculations, not structure optimisation in contrast to its canonical counterpart.

Even though canonical CC methods provide very reliable structures (e.g., for organic molecules), it is recommended in few cases to solely rely on this method, as the computational cost becomes very high with increasing system size. Therefore, other methods like density functional theory, perturbation theory or semiempirical methods play a big role in modern computational chemistry.

1.2.2 Density Functional Theory

It was proven by Hohenberg and Kohn in 1964, that the energy of a system can be solely described as a functional of the **electron density**. The beauty of this approach is that in principle the electron density can be described by only three coordinates (x,y,z) in contrast to the wave-function-based methods, where three coordinates for each electron lead ultimately to a more complicated case of 3N coordinates for N electrons in total. Unfortunately, the functional to accurately connect electron density to the corresponding energy remains to be found.[43]

The **Kohn-Sham** (KS) formalism of DFT provides an accurate density functional (E_{KS}) except for the exchange (E_x) and the correlation energy (E_c) of the system. Since those make up only a small part of the total energy, the KS model by itself managed to provide relatively accurate results, which led to a rise in popularity of DFT.[49–51]

$$E_0 = E_{KS} + E_X + E_C \tag{4}$$

To compensate for the missing electron exchange energy, **hybrid functionals** were introduced, which add varying amounts of Hartree-Fock exchange to DFT methods, as the electron exchange energy is accurately described in HF.[52,53] One of the most famous of these hybrid functionals is B3LYP,[54] which serendipitously showed very good results on a wide range of organic systems by including twenty percent HF exchange energy.[55,56]

1.2.3 Dispersion, Solvation, Conformational and Transition State Search

Dispersion forces, also known as London forces, are intermolecular interactions of temporary induced dipole moments of molecules at intermediate distances, creating an attractive force.[43] Especially in large systems and systems containing delocalised electrons, these interactions play a crucial role for the energy of the investigated system. A lot of research still focuses on the development of new cost-effective methods that can accurately describe these interactions in density functional calculations.[57,58] While the group of Grimme has developed the very reliable dispersion correction method D3, it was still improved by a revision of the BJ-damped variants by Sherill and co-workers in the D3BJ version.[59–61] Important examples of these non-covalent interactions include attractive forces of saturated hydrocarbons and π-stacking of benzene rings (Figure 12).

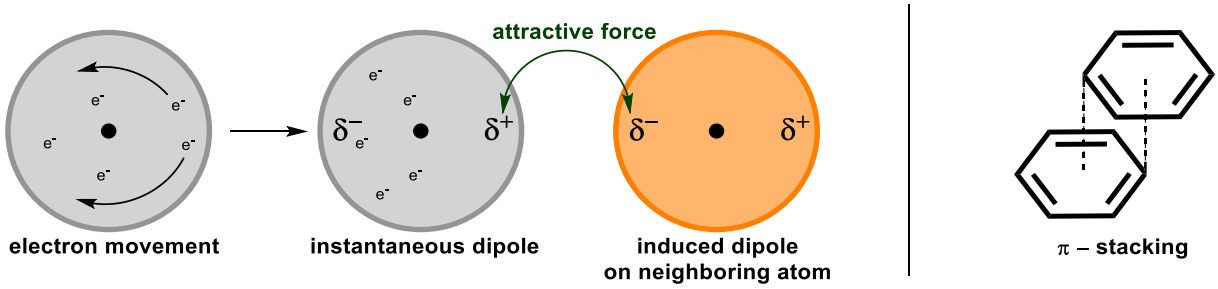

Figure 12: Graphical explanation of dispersion effects and the most prominent example: π-stacking

Solvation effects play a major role in the investigation of reactions since most reactions are conducted in solution. Computationally, there are two approaches of solvation, explicit and implicit solvation. The former is considered in e.g., QM/MM-MD (quantum mechanics/molecular mechanics molecular dynamics), in which the movement of the independent solvent molecules is simulated (Figure 13, right).[62,63] For quantum chemical calculations that is hardly feasible due to the high computational cost, which is why approaches, describing the solvent as a continuous medium encasing the solutes, are favoured. An example for this is the self-consistent reaction field model (SCRF), in which a solvent cavity containing the solute is created within a polarisable solvent shell. Polarisability in this case means that the charge of the solute molecule induces the dipole moment of the solvent shell, which in turn affects the wave function of the calculated molecule.[40,43]

Standard methods for implicit solvation, implemented in most quantum chemical programs, include the polarised continuum method (PCM, Figure 13, left)[47,64] and the related conductor-like polarisable continuum model (CPCM),[65,66] which both have been proven in benchmark experiments to yield reliable results. An improvement upon PCM came with the introduction of the solvation model based on molecular electron density (SMD),[67] which includes neglected aspects of PCM like the cavity creation in the continuous solvent and attractive solute-solvent dispersion interactions.

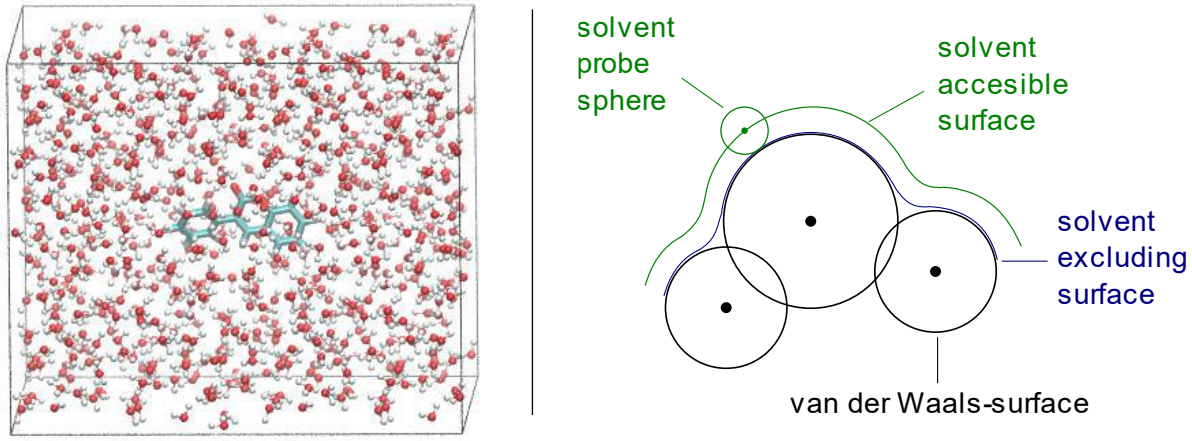

Figure 13: Molecular dynamics simulation of coumarin in water by Kumar et. al. (left) and Graphical explanation of PCM solvation model: solvent probe spheres along the solvent excluding surface create the solvent accessible surface (right)

Especially for large and flexible molecules, the investigation of the conformational space of a molecular system plays a major role when comparing energies. To keep computational cost low, most approaches for **conformational search** use semi-empirical or force-field methods. In this project, both the semiempirical extended tight-binding (GFN-xTB) method and the force-field (GFN-FF) method as implemented in the Conformer-Rotamer Ensemble Sampling Tool (CREST) by Grimme and co-workers were applied and compared.[68,69]

Conformational search results in a vast number of generated structures, with corresponding energies supplied by the force-field method (Figure 14, **A**). Due to the low accuracy of semi-empirical or force-field methods, the energy is recalculated using DFT to determine the most stabilised conformations (Figure 14, **B**). Usually, an energy threshold (e.g., 7 kcal/mol) is used to determine which conformations would be optimised by DFT. In this project however, only the 6 most stable conformations were used for further optimisation, due to the system size and the limited time, followed by single point calculation at higher level of theory (Figure 14, **C, D**). The conformational search is essential because it allows localizing the most stable structure (conformer). Moreover, in some cases, it is crucial to take the whole conformational

space into account by Boltzmann averaging (see 3.1.6 The Boltzmann Averaged Gibbs Free Energy Calculations).

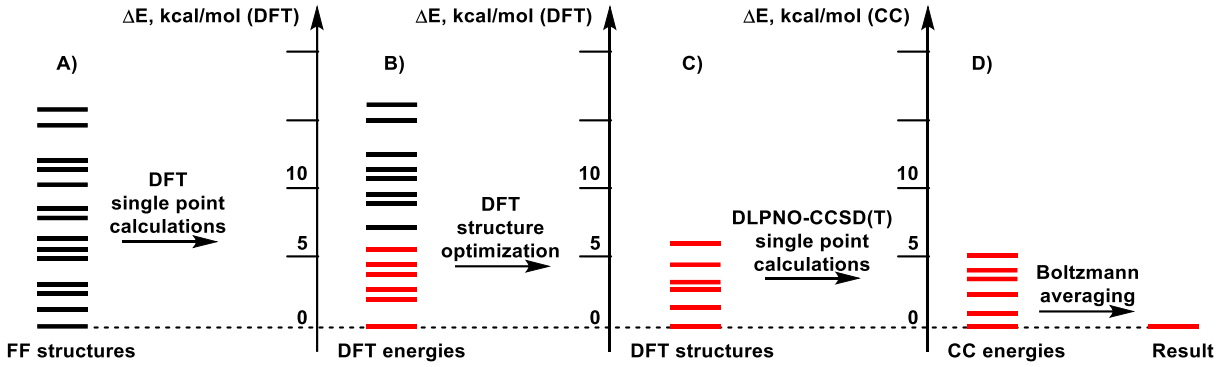

Figure 14: Graphical depiction of conformational search procedure

The **nudged elastic band** (NEB) method is a widely used approach for finding elusive transition state geometries.[70,71] Using the initial and final geometry of a transformation, the method constructs a minimum energy pathway by creating replicas of the system (usually 4-20 structures) interpolating the reaction coordinate (Figure 15).[72] To assure the continuation from one structure to the next, an elastic band interaction connects adjacent interpolation points. The optimisation of each of these structures leads to an energy curve showing a maximum near the interpolation structures that resemble the corresponding transition state. Upon optimisation of the structures near the interpolated maximum, it is usually possible to locate the transition state, if this fails however, more interpolations can be applied.

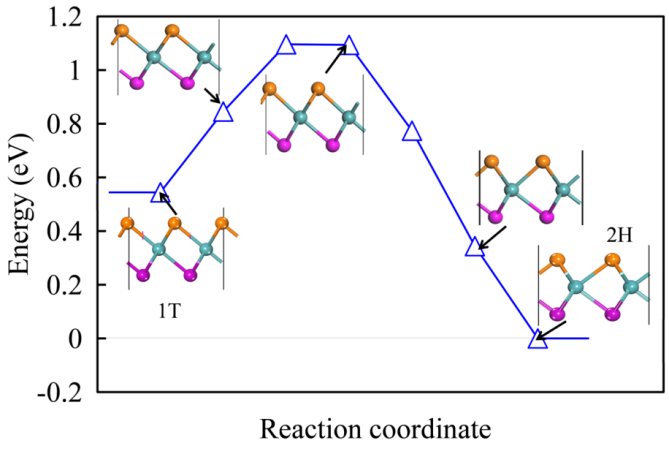

Figure 15: Example of a nudged elastic band calculation by Mortazavi et. al.[71]

2. Objectives of the Thesis

Computational investigations were employed to further understand the diastereoselectivity of the previously reported 1,4-dicarbonyl synthetic method (Figure 16). Considering the proposed reaction mechanism, the difference in d.r. should be explainable by comparing the energies (ΔG) of the corresponding chair (TS_A) and boat (TS_B) transition states of the rearrangement (Figure 16). The aim of the computational study was to investigate the energy barriers leading to the different diastereomers, hereby explaining unexpected experimental outcomes and increasing the overall understanding of the underlying mechanism.

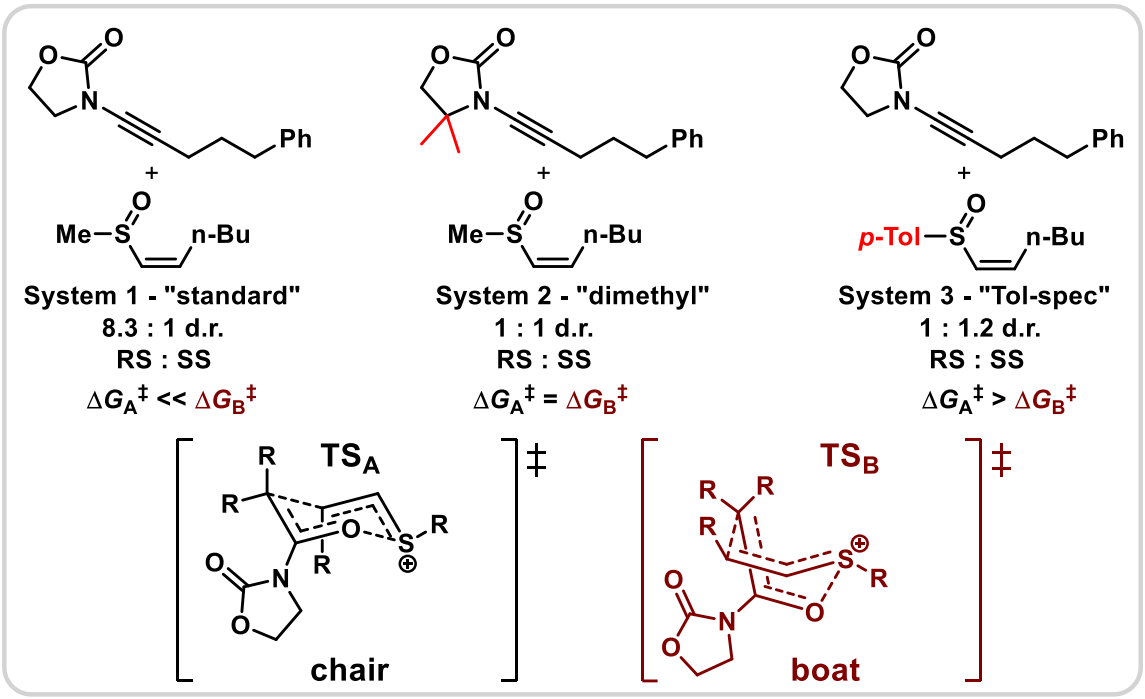

Figure 16: Systems chosen for the computational study

The resulting 1,4-dicarbonyl compounds were also investigated for their reactivity with different nucleophiles, to access lactones and lactams with a high degree of diastereomeric control. In these transformations a third chiral centre can be formed. The diastereocontrol of this event is highly depended on the substitution pattern around the formed heterocycle and the reaction parameters, both of which were the subject of my study. (Figure 17)

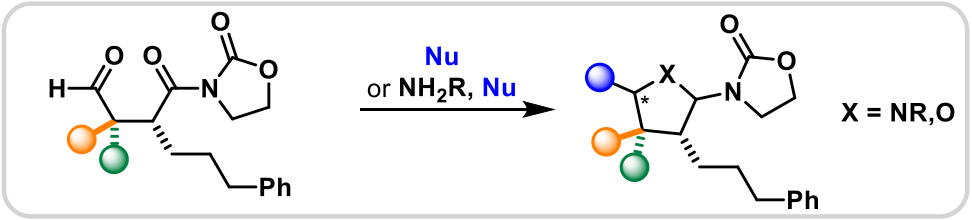

Figure 17: Investigation of 1,4-dicarbonyl applications

3. Results and Discussion

3.1. Computational Investigation of Diastereoselectivity

3.1.1 Computational Details

The proposed structures were constructed using GaussView[73] and subjected to B3LYP/def2-SVP geometry optimisation. The conformational space of the resulting molecules was searched using meta-dynamics simulations based at the GFN-xTB and GFN-FF levels of theory as implemented in CREST 2.11.[69]

Single point calculations of the obtained conformations were conducted at the B3LYP/def2-SVP level of theory, after which the three most stable conformations were reoptimised. Finally, single point energies of the reoptimised structures were calculated at the DLPNO-CCSD(T)/def2-TZVP and B3LYP/def2-TZVP level of theory. The thermal corrections to the Gibbs free energy, calculated after the geometry optimisation, were combined with the coupled-cluster single point energies to yield the Gibbs free energies ("G_{273}") at 273.15 K. The solvation model based on the molecular electron density (SMD) and the conductor-like polarisable continuum model (CPCM) were used to consider the solvent effects of dichloromethane (DCM) during the geometry optimisation and the single point calculations respectively. D3BJ dispersion correction was used for all DFT calculations.[61]

The DFT calculations were performed using Gaussian 16.[74] The coupled-cluster calculations were performed using ORCA.[75,76] The nudged elastic band (NEB) as implemented in the Turbomole program package[77] was used to find nontrivial transition states.

To determine the transition states of the reaction mechanism, the corresponding bond vibration frequencies were calculated. Transition states generally show high imaginary frequencies along the reaction coordinate. Method and corresponding basis set are denoted by using a slash between level of theory and basis set (e.g., B3LYP/def2-SVP) or when using a different method for optimisation than energy calculation, they are separated by two slashes, with the method and basis set for the energy going first (DLPNO-CCSD(T)/def2-TZVP//B3LYP/def2-SVP).

3.1.2 Investigation of Cationic Systems

Three systems were investigated to improve the understanding of the reactions' diastereoselectivity. **System 1 – "standard"** (Figure 18, **A**, left) was used as the reference, as it experimentally showed good diastereoselectivity. On the other hand, the addition of two geminal methyl groups to the oxazolidinone (**System 2 – "dimethyl"**, Figure 18, **A**, middle), as well as the use of a *para*-tolyl (*p*-Tol) group as a spectator ligand (see chapter 1.1.2) on the vinyl sulfoxide (**System 3 – "Tol-spec"**, Figure 18, **A**, right) both led to complete loss of selectivity. To reduce the computational cost, some simplifications were applied by cutting the size of the studied molecules. The aromatic side chain of the ynamide was shortened to a methyl substituent, while the *n*-butyl vinyl sulfoxide was replaced by the ethyl vinyl sulfoxide (Figure 18, **B**).

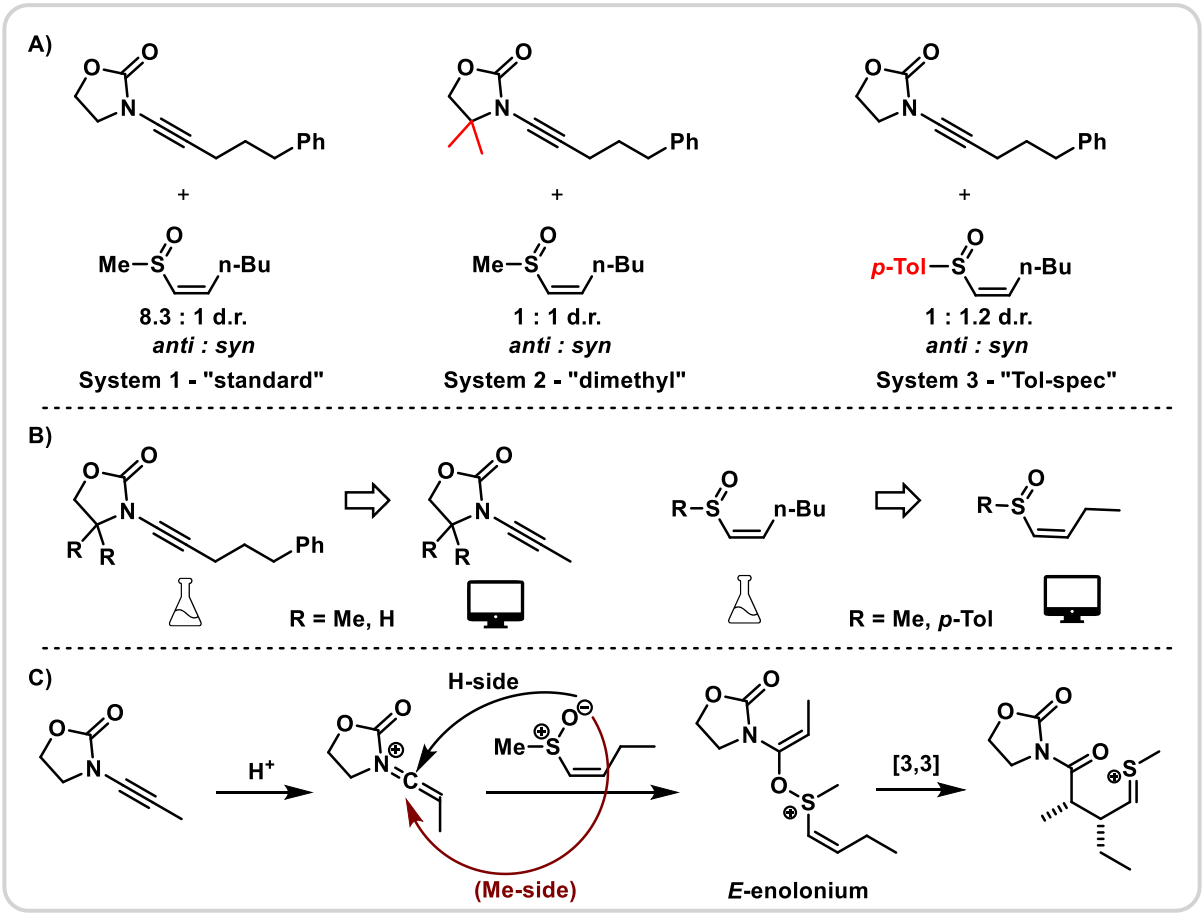

Figure 18: A) Systems with counterintuitive experimental results. B) Structural simplifications applied to reduce computational cost. C) Proposed reaction mechanism involving nucleophilic attack from the H-side.

The first step of the proposed reaction mechanism (Figure 18, **C**) is an activation of the ynamide by a Brønsted acid, forming the corresponding keteniminium ion. The effect of the hereby deprotonated acid counterion is investigated in 3.1.3 Counterion Consideration. To keep computational cost low for the first investigation, it was conducted without the counterion. The attack of the vinyl sulfoxide on the easily accessible hydrogen side of the keteniminium ion, leading to the *E*-enolonium (Figure 18, **C**, R_1=H; R_2=Me) was considered, as well as the sterically more challenging alternative, leading to the *Z*-enolonium (Figure 18, **C**, R_1=Me; R_2=H) (see 3.1.5 Sulfoxide Addition for more details). For the sigmatropic rearrangement, all 4 conceivable transition states, with a chair and boat for both pseudo-axial and pseudo-equatorial orientations of the spectator ligand were considered. Additionally, both enolonium geometries were investigated, leading to 8 transition state diastereomers (Figure 19).

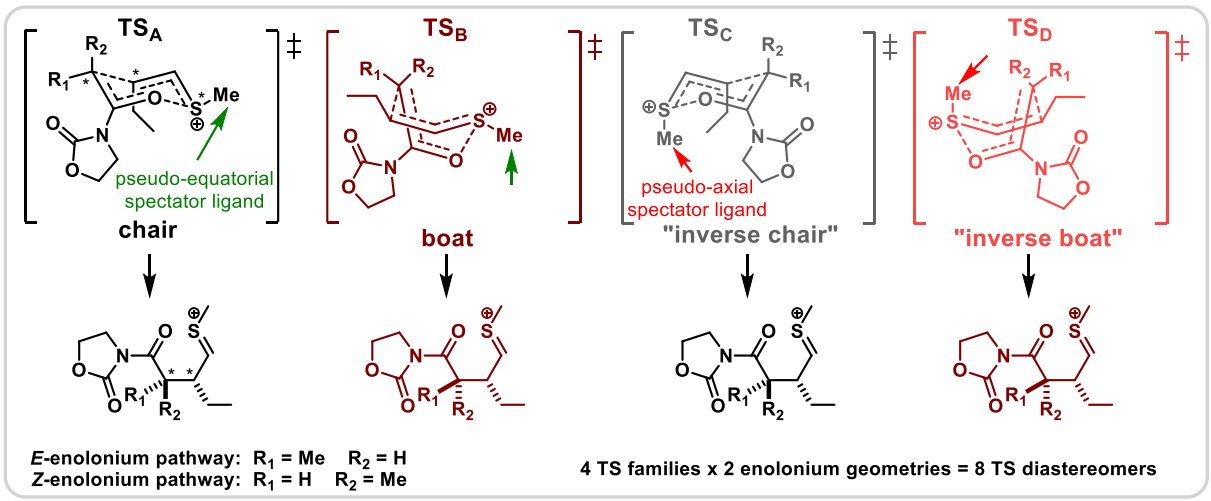

Figure 19: Structure of the 8 possible transition state diastereomers

These preliminary results indicate that the inverse transition states, with an axial spectator ligand (**TS_C, TS_D**), are massively disfavoured (ΔG = 13.0-16.8 kcal/mol, Figure 20), as would be predicted by the Zimmermann-Traxler model, which is why no further investigation was conducted on those pathways. The *Z*-enolonium inverse chair transition state (**$TS_{D\text{-}Z}$**) did not converge during optimisation with SMD implicit solvation, gas-phase calculations show a very high energy barrier, thus this type of transition state was neglected.

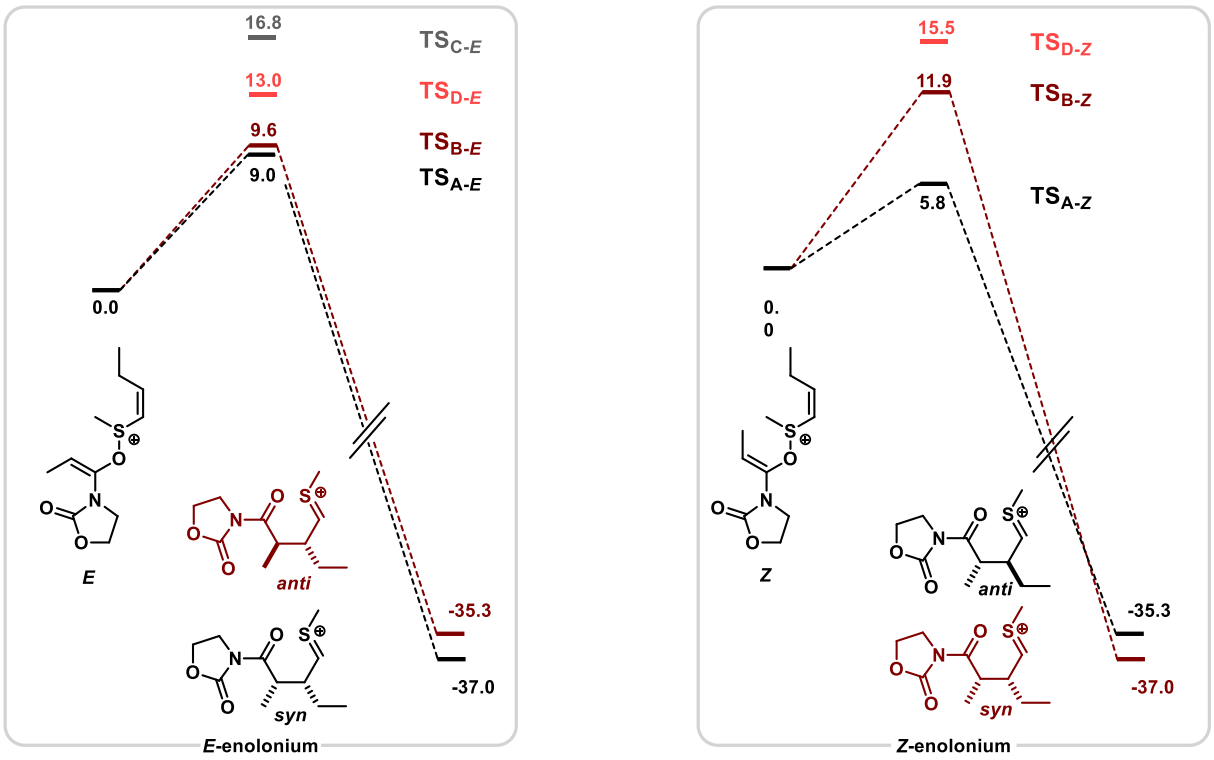

Figure 20: Computed free energy profiles without counterion effects at the DLPNO-CCSD(T)-CPCM/def2-TZVP//B3LYP-D3BJ-SMD/def2-SVP level of theory, $\Delta G_{273,\,DCM}$ in kcal/mol. The enolonium intermediate was used as reference (0.0 kcal/mol)

Unexpectedly, the chair conformation of the transition state after Me-side attack is the most stabilised one (Figure 20, **TS$_{A-Z}$**). This would indicate the formation of the opposite diastereomer than observed in the experiment. We have investigated this counterintuitive computational result in detail in chapter 3.1.5 Sulfoxide addition.

These preliminary results showed the problem complexity, requiring further considerations.

3.1.3 Counterion Consideration

Previous studies[37] show that counterions play an essential role for the enantioselectivity of sulfonium rearrangements. Inspired by both experimental and computational results from our group, we decided to augment our calculations by adding counterions to the system.

In the experiment, the superacid bis(trifluoromethane)sulfonimidic acid, also known as bistriflimide (**Tf$_2$NH**, Figure 21, left) was used to activate the ynamide. As Tf$_2$NH is very flexible

and can access a large number of conformations, dramatically increasing the computational cost of the study, a simplification was employed by using the cyclic hexafluoropropane disulfonimide (Figure 21, right), which leads to very similar experimental results but covers a much smaller conformational space due to cyclic rigidity. This cyclic acid and corresponding anion will be abbreviated in the following as "Tf_2NH" and "Tf_2N^- "respectively.

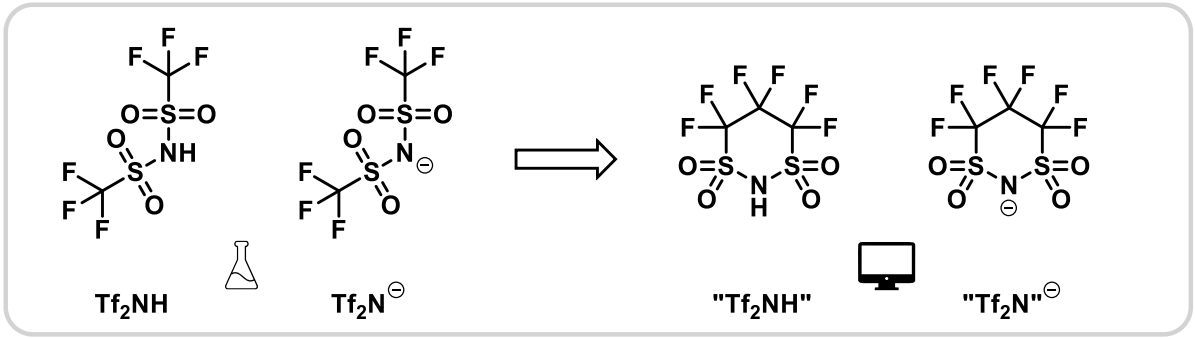

Figure 21: Lowering the structural flexibility of the superacid and corresponding counterion to reduce the computational cost

The previously discovered geometries for the cationic forms of the intermediates and transition states were now extended by inclusion of the counterion and reoptimised. The resulting structures were subjected to xTB conformational search and reoptimised (Figure 22). In this series of computations, the chair-like sigmatropic rearrangement of the *Z*-enolonium intermediate is still the favoured TS in each system (Figure 22, $\mathbf{TS_{A\text{-}\mathit{Z}}}$) and the chair-boat energy difference of **System 3** is bigger than expected ($\Delta\Delta G^{\ddagger}$ = 1.4 kcal/mol). As the experimental observations show a much smaller energy difference, more thorough investigation was required.

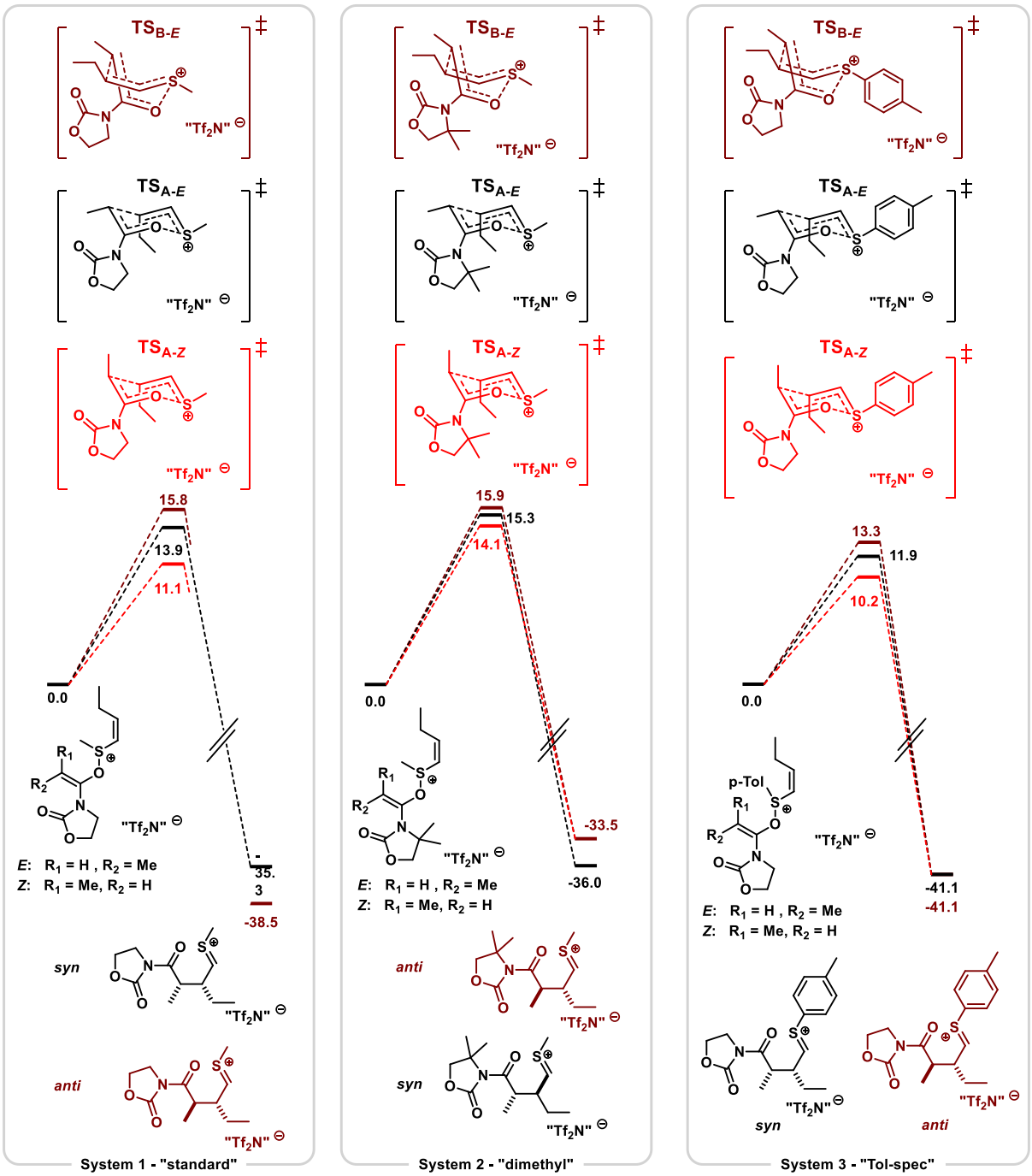

Figure 22: Computed Gibbs free energy profile for neutral systems (including counterion) at the DLPNO-CCSD(T)-CPCM/def2-TZVP//B3LYP-D3BJ-SMD/def2-SVP level of theory, $\Delta G_{273,\,DCM}$ in kcal/mol. The enolonium is used as reference (0.0 kcal/mol)

3.1.4 Conformational Search Approaches: xTB vs. GFN-FF

We have compared two different approaches for the conformational exploration of the considered systems: semiempirical GFN-xTB and the GFN-FF force field methods. The results show substantial discrepancy between the exploited approaches. During the conformational search using xTB, some structures formed covalent adducts of the counterion to the cationic

sulfonium species (Figure 23). However, upon subsequent DFT optimisation, the covalent bond was broken to reform separated ions. Since DFT is a more reliable method, the covalent bond appears to be an artifact of the semi-empirical approach xTB. As the covalent bond drastically reduces the degrees of freedom for rotation and prohibits displacement of the counterion, only a very limited number of conformations could be found, which made the need for a different method evident.

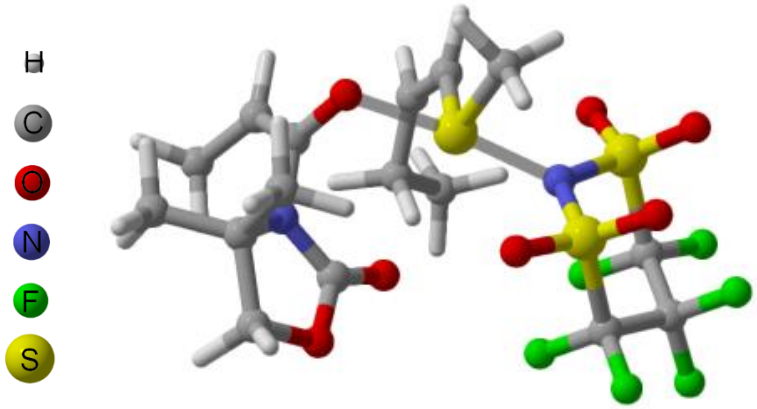

Figure 23: Covalent adduct of counterion to sulfur atom during xTB conformational search

After this discovery, another conformational search was conducted using the force field approach GFN-FF. Even though a lower transition state for all *E*-enolonium transition states was found, due to the enhanced conformational space exploration, the lowest reaction barrier was still found to originate from the *Z*-enolonium chair transition state $\mathbf{TS}_{\mathbf{A}\text{-}\mathit{Z}}$, which would lead to the experimentally unobserved diastereoselectivity. Therefore, more thorough investigation of the sulfoxide addition event was conducted.

3.1.5 Sulfoxide Addition

The steric preference of the sulfoxide addition plays an essential role in the reaction outcome, as the inversion of the adduct geometry leads to the inversion of the diastereoselectivity. The investigation of the corresponding transition states was far from trivial, as there were significant convergence problems for the *E*-addition of the sulfoxide. To obtain the transition states, a method called nudged elastic band (NEB) was applied, which interpolates the reaction coordinates of two minima to find the connecting transition states. The resulting

energies indicate a selectivity contrary to chemical intuition, favouring the more sterically hindered *Z*-enolonium formation for all three investigated systems.

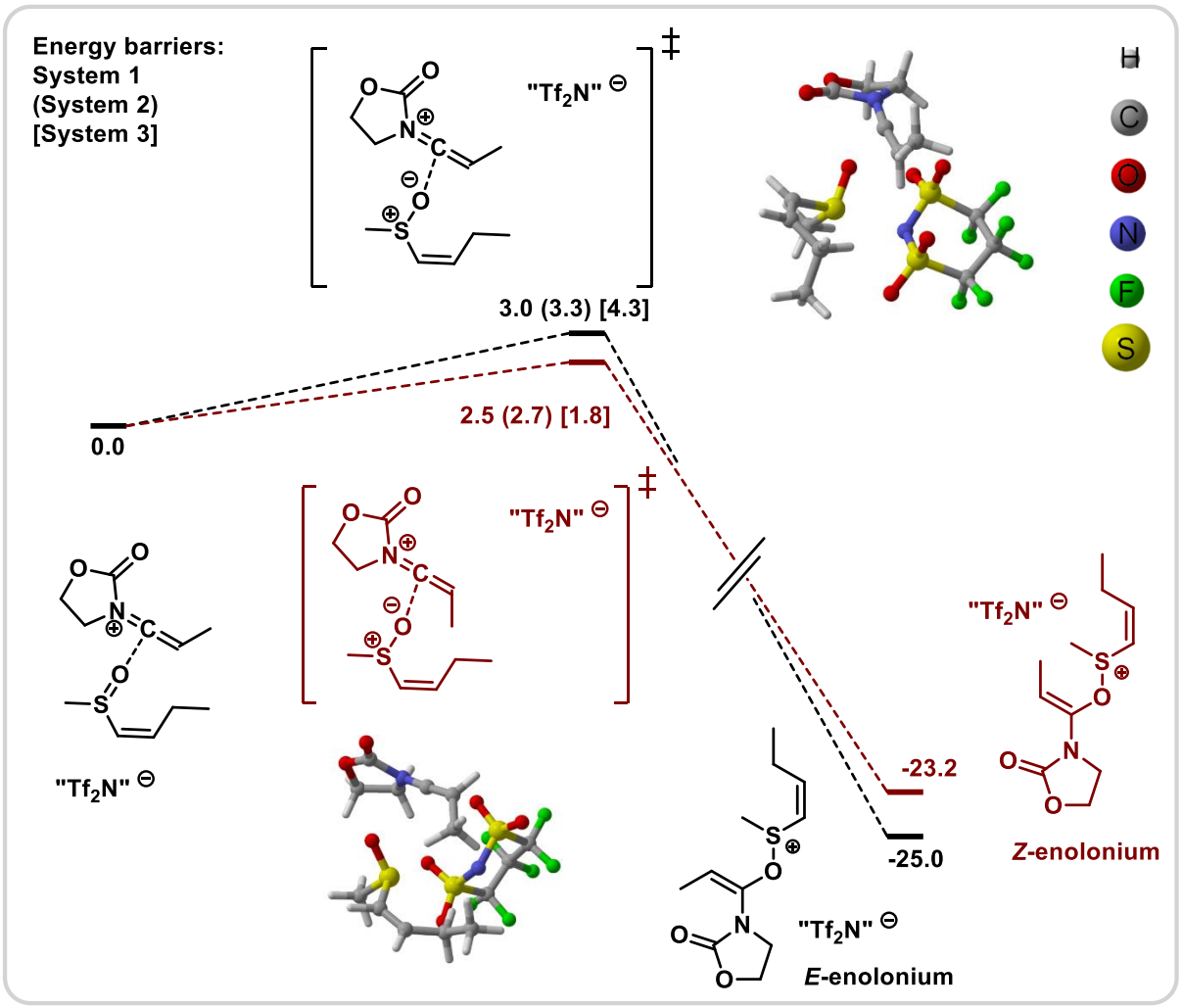

Figure 24: Computed Gibbs free energy profile of the two possible sulfoxide attack pathways for System 1, System 2 (energy values in brackets) and System 3 [energy values in square brackets]. Level of theory: DLPNO-CCSD(T)-CPCM/def2-TZVP//B3LYP-D3BJ-SMD/def2-SVP level of theory, $\Delta G_{273,\,DCM}$ in kcal/mol

Notably, all computed reaction barriers for this transformation are very low (~2-3 kcal/mol, Figure 24), meaning a reaction will take place as soon as the reactants are in proximity. Considering the high electron density at the oxygen of the vinyl sulfoxide, increased by the partial S-O single bond character, it can be plausible that before the formation of the keteniminium, the acid will protonate the vinyl sulfoxide first (Figure 25), followed by proton transfer to the ynamide. After this transfer, the sulfoxide would already be present in immediate proximity for the nucleophilic attack, which happens immediately due to the low barrier, favouring the *E*-enolonium formation.

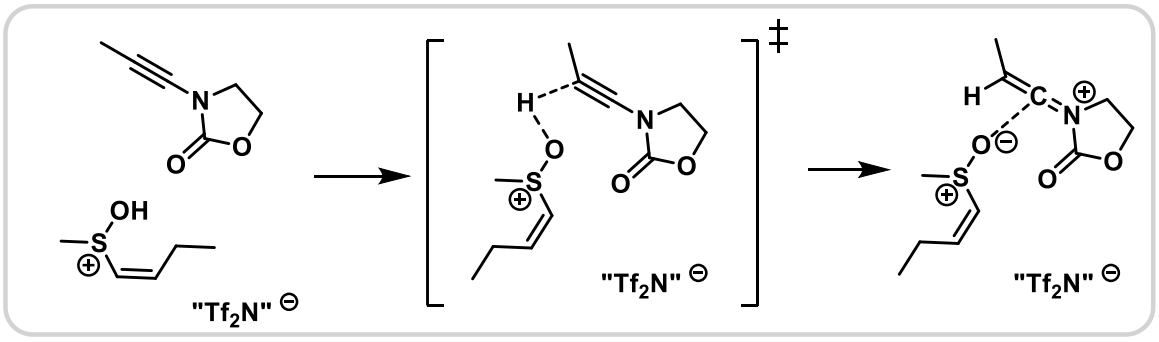

Figure 25: Possible reaction pathway via sulfoxide protonation before keteniminium formation

To test this hypothesis, several calculations were performed. Regarding the protonation event an energy scan was conducted, showing that there is close to no barrier for the sulfoxide protonation (Figure 26), while a barrier of 9.9 kcal/mol was calculated for the protonation of the ynamide by "Tf_2NH". The search for the transition states for the protonation of the ynamide by the protonated sulfoxide, as well as for a concerted reaction were unsuccessful. Possibly more thorough investigation can produce a clearer answer, the investigation was cut short due to the limited time frame of the thesis, however.

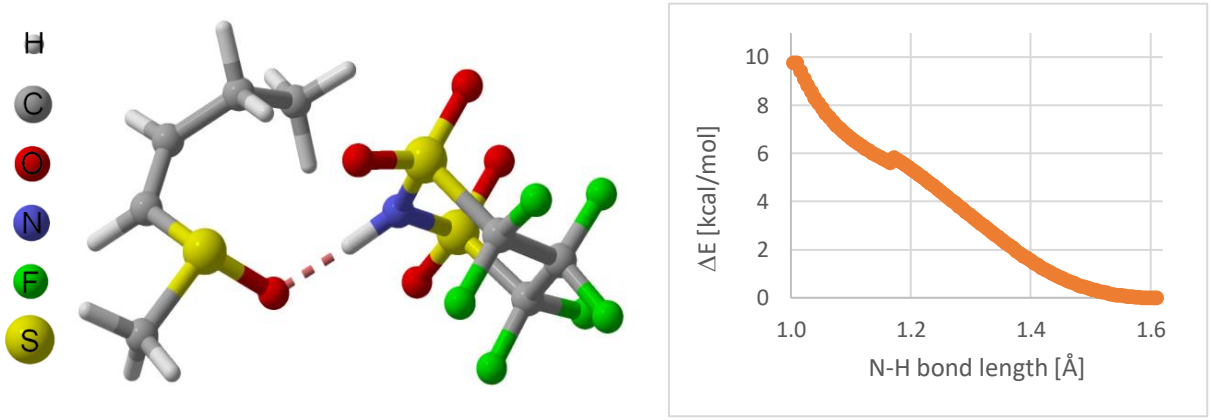

Figure 26: The optimized structure of the sulfoxide and superacid complex (left) and the energy scan of sulfoxide and superacid shows close to no barrier for sulfoxide protonation (right)

The addition to an ynamide with a bulkier substituent was then investigated, as it better resembles the experiment (Figure 27). An addition on the *E*-side was postulated to be more favoured with bulkier substituents, however, initial results still showed a preference for the bulky side. In parallel, experimental associates managed to perform the transformation with good selectivity also for methyl ynamides, showing the reaction's independence of this substituent.

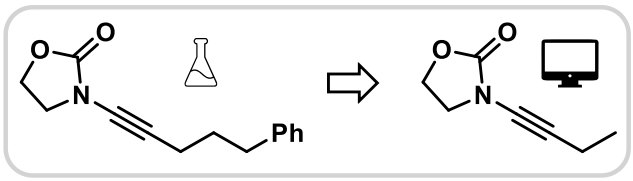

Figure 27: Attempt to approach experimental conditions by using less simplification

Due to the above-mentioned considerations and the energy scan reinforcing the hypothesis, the Me-side formation and the corresponding rearrangement transition state were neglected. Subsequently, the selectivity would be dictated by the chair and boat transition states of the *E*-enolonium intermediate.

3.1.6 The Boltzmann Averaged Gibbs Free Energy Calculations

To have a more accurate result, which takes into account more conformations than only the most stable, Boltzmann averaging was applied. This approach weights the different conformations according to their relative energies to the most stable conformation (G_{min}) (5, left) and averages the total energy according to the following equation (5, right):

$$p_i = \frac{e^{-G_i - G_{min}}}{\sum e^{-G_i - G_{min}}} \qquad G_{avg} = \sum p_i * G_i \tag{5}$$

The Boltzmann averaged final energy differences of the corresponding chair and boat transition states (Figure 28) are shown in Table 1 for different levels of theory. Additionally, the experimental energy difference calculated according to the Eyring equation (6, left) is added for comparison.

$$k = \frac{k_B T}{h} * e^{-\frac{\Delta G^{\ddagger}}{RT}} \qquad d.r. = \frac{k_1}{k_2} = e^{-\frac{\Delta\Delta G^{\ddagger}}{RT}} \tag{6}$$

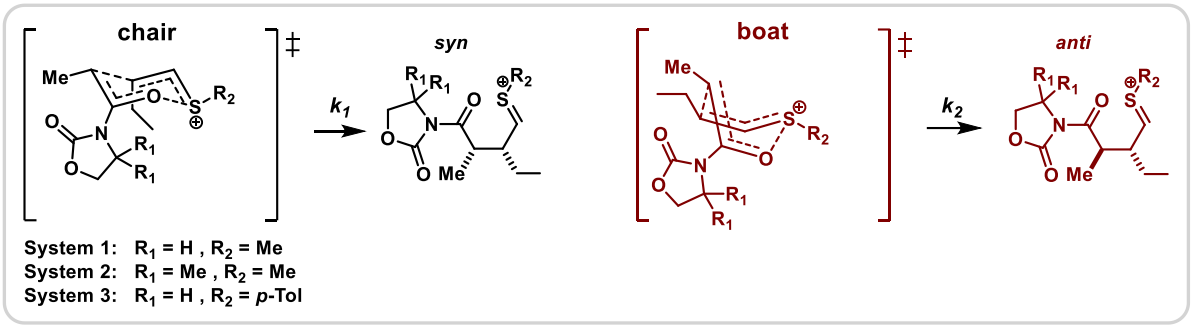

Figure 28: Compared transition states and corresponding product geometries

Table 1: Boltzmann averaged energies of low energy conformations calculated at different levels of theory, colour-code for error: >1: red, ≤1 yellow, ≤0.5 pale green, ≤0.1 green, all energy differences in kcal/mol at 273.15 K in DCM

	d.r.$_{exp}$	$\Delta\Delta G^{\ddagger}_{exp,\ calc.}$ [a]	$\Delta\Delta G^{\ddagger}_{calc.\ M1}$ [b]	$\Delta\Delta G^{\ddagger}_{calc.\ M2}$ [c]	$\Delta\Delta G^{\ddagger}_{calc.\ M3}$ [d]
System 1	8 : 1	~ -1.1	-3.2	-1.6	-0.4
System 2	1 : 1	~ 0	-1.8	-2.7	-0.3
System 3	1 : 1.2	~ 0.1	1.1	-2.9	0.2

[a] Calculated using the experimental d.r. and the equation (5).
[b] Computed at the B3LYP-D3BJ/def2-SVP level of theory (method M1).
[c] Computed at the B3LYP-D3BJ/def2-TZVP//B3LYP-D3BJ/def2-SVP (method M2).
[d] Computed at the DLPNO-CCSD(T)/def2-TZVP//B3LYP-D3BJ/def2-SVP (method M3).

While on the highest level of theory M3, **System 3** shows excellent correlation of calculation and experiment, the energies of **System 1** and **2** show slightly higher deviation from expected values, a general trend towards the experimental values is recognisable, however. Comparing to other calculations, the overall agreement for the Boltzmann averaged DLPNO-CCSD(T) energy gives the best results, as expected.

3.1.7 Outlook

In this section, the various approximations and simplifications, general considerations of the result accuracy and unexpected outcomes will be discussed. Due to the complexity of the investigated system, none of these considerations are trivial and no claim to completeness is laid.

The **accuracy** of modern quantum chemical methods is limited to approximately 1 kcal/mol in best case scenarios. In the investigation of diastereoselectivity, a very small difference in energy can result in substantial change in the corresponding d.r., as shown in Table 1. The moderate agreement between the experimental and computational results can therefore be connected with the accuracy of the quantum chemical approach.

During the conformational search of the sulfonium rearrangement product (Figure 29, **A**), a peculiar, substituted **tetrahydrofuran (THF) derivative** (Figure 29, **B**) was detected, for conformations in which the amide oxygen comes into proximity of the sulfonium carbon. Due to the high electron density of the amide oxygen and the strong electrophilicity of the sulfonium carbon, the cyclisation appears to be barrierless. This unexpected species could be a source of epimerisation, due to the very acidic proton on the chiral centre.

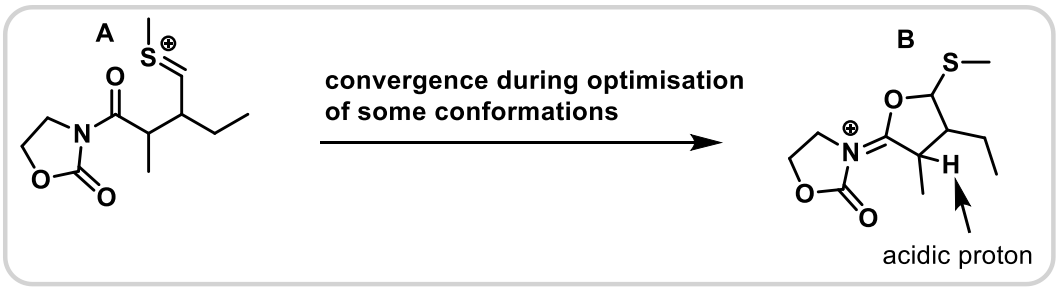

Figure 29: Conformations of the sulfonium rearrangement product, in which the carbonyl oxygen comes in proximity to the sulfonium carbon leading to THF derivatives

Experimentally, the reaction is conducted in the presence of an excess of water to hydrolyse *in situ* the sulfonium intermediate. All calculations were carried out without taking the water into account, which is a major approximation, as all intermediate structures are charged and therefore possess high water affinity. Calculations with explicit water molecules can be conducted, but the complexity of the resulting system grows substantially. Considering the

very reactive charged intermediates, water adducts could play a big role until the irreversible sulfonium hydrolysis. An excess of isobutyraldehyde is also added to the reaction mixture to avoid an attack of the thiol, which is released upon hydrolysis, on the product. This reagent was also not considered during the computational studies, since an interference with the rearrangement is unlikely.

To increase the level of approximation to the experiment, the three systems were also investigated without the implemented structural simplifications mentioned in the beginning of 3.1.2 Investigation of Cationic Systems (Figure 30). Initial results of this investigation show a similar outcome to the systems using shortened substituents. A full conformational search could not be conducted due to time limitations, as the optimisation of the massively enlarged molecules requires a lot of computational time.

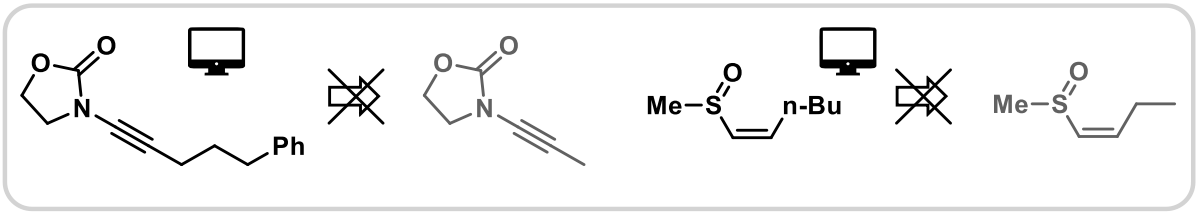

Figure 30: Investigated systems without simplification to reduce calculation time

3.2. Experimental Investigation of Potential Applications

3.2.1 1,4-Dicarbonyl Synthesis

To find applications for the previously discovered 1,4-dicarbonyl synthesis, an array of different starting materials needed to be prepared. Using the procedure published by the Maulide group in 2018,[39] it was possible to obtain 1,4-dicarbonyls with high diastereoselectivity (Figure 31). Since the chirality transfer was thoroughly investigated before, racemic vinylsulfoxides were applied.

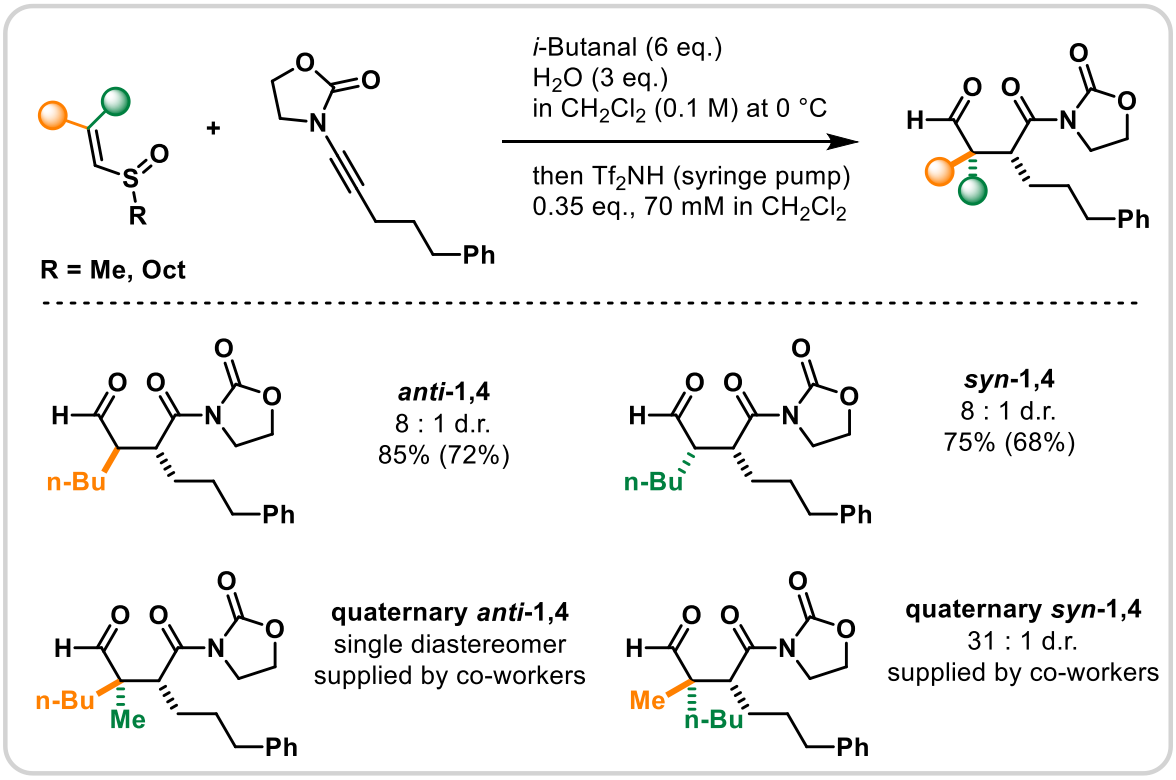

Figure 31: Synthesis of 1,4-dicarbonyls used for further transformations

The resulting 1,4-dicarbonyl compounds were treated with different nucleophiles to explore the potential for γ-substituted lactam and lactone synthesis. Additionally, hydrazine nucleophiles were also investigated, resulting in pyridazine formation.

3.2.2 Lactam Synthesis

Starting from the previously synthesised 1,4-dicarbonyl aldehydes, γ-unsubstituted cyclised lactams (**8**) can be easily accessed by addition of an amine, followed by reduction. The reaction was thoroughly investigated by Alexander Beaton, Uroš Todorović and Dr. Margaux Riomet (Figure 32, **A**). Additionally, the acyl iminium intermediate can be trapped by a second nucleophile, namely an allyl silane (Figure 32, **B**) affording the corresponding γ-allyl lactam (**9**).

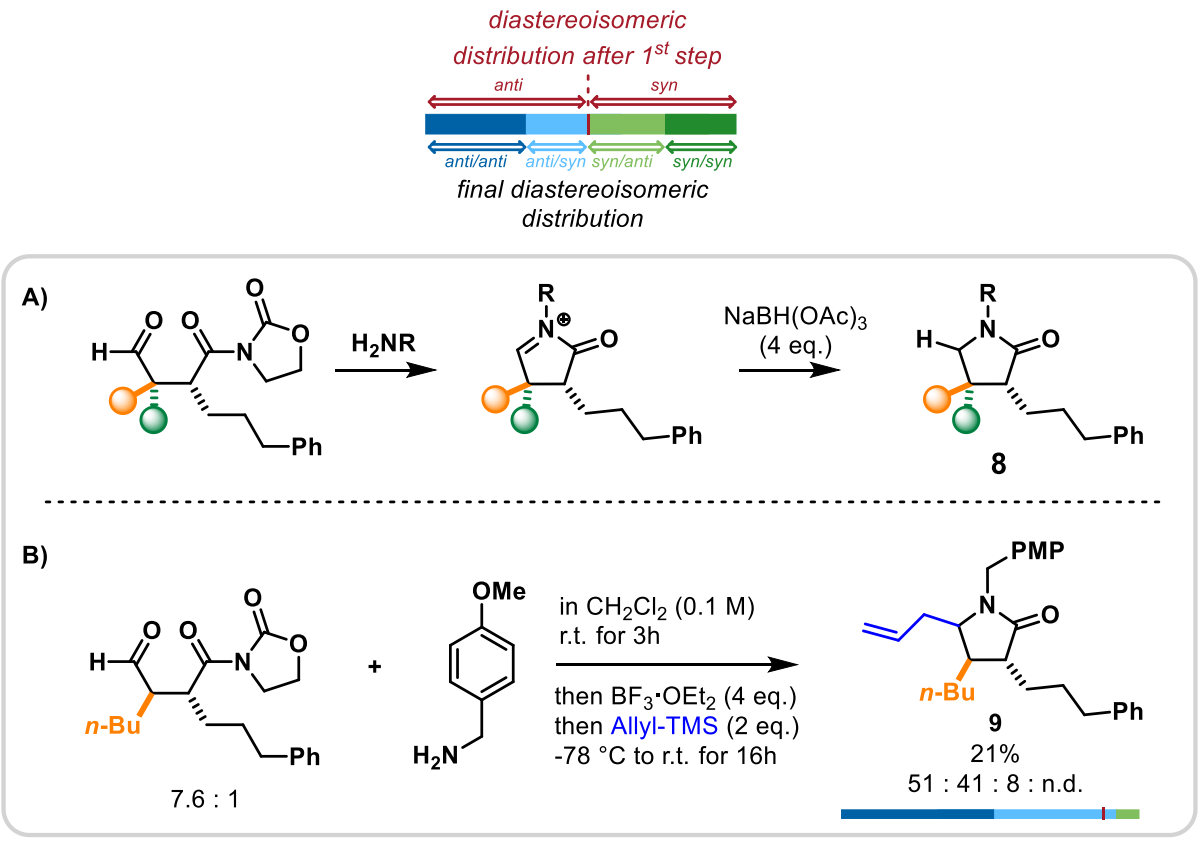

Figure 32: γ-unsubstituted (A) and γ-substituted (B) lactam synthesis

In order to obtain complex structures, an internal nucleophile can be employed. An array of bisnucleophiles were screened on an analytical scale, followed by LCMS analysis.

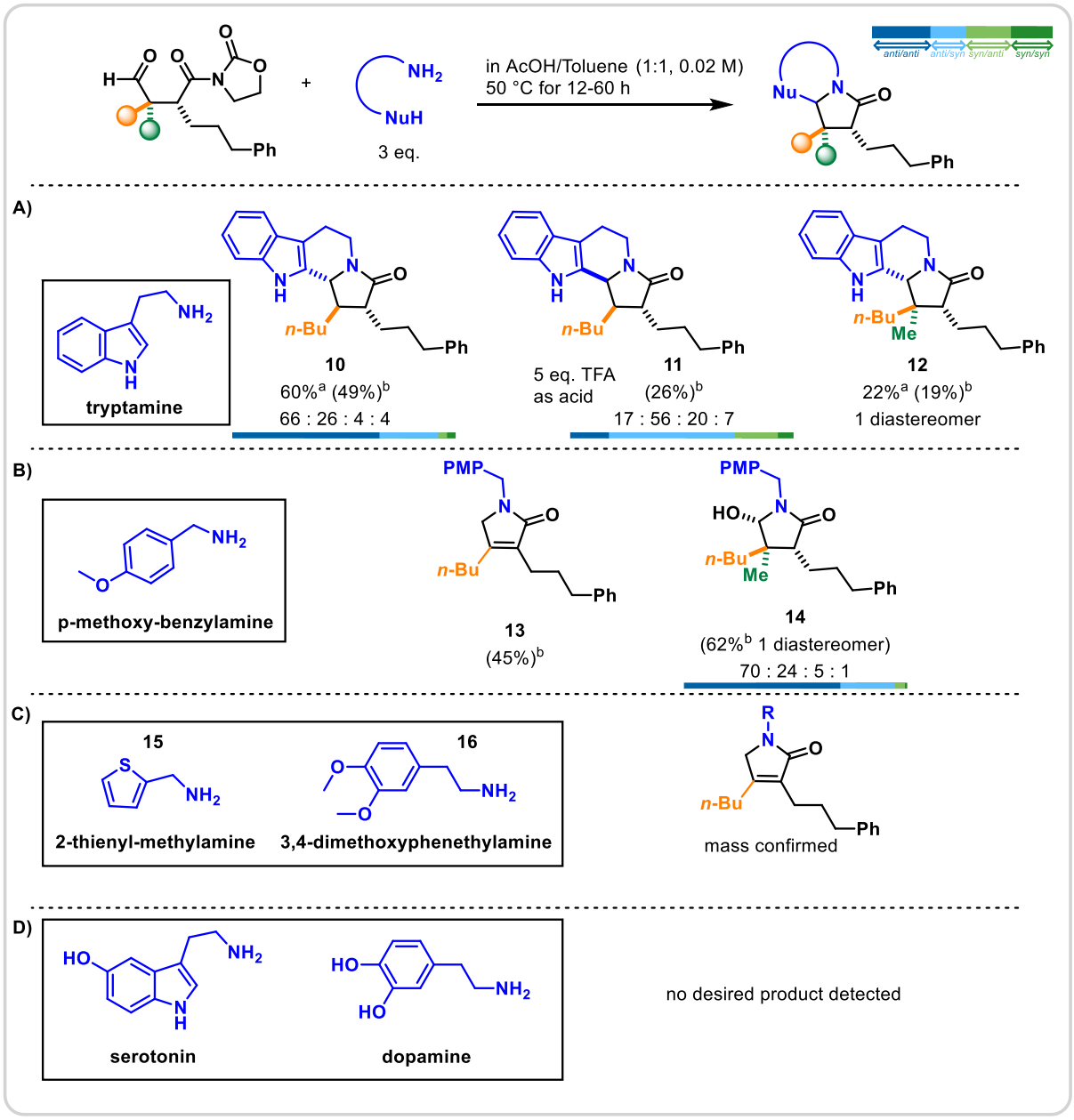

Figure 33: Investigation of different potential bisnucleophiles in the synthesis of γ-substituted lactams, [a] NMR yield. [b] isolated yield.

Among the investigated candidates for polycycle formation, only tryptamine (Figure 33, **A**) was able to react as desired to produce polycyclic products (**10**). While the thermodynamically favoured *anti-anti* product is the major diastereomer using acetic acid, an opposite selectivity for the newly formed stereocentre could be achieved by employing 5 equivalents of trifluoroacetic acid (TFA) in toluene. When using acetic acid, significant epimerisation occurs, possibly by deprotonation in the β-position (Figure 34, **A**). This assumption is reinforced by experiments showing identical d.r. for 1,4-dicarbonyl starting materials with varying d.r. (Figure 34, **B**)

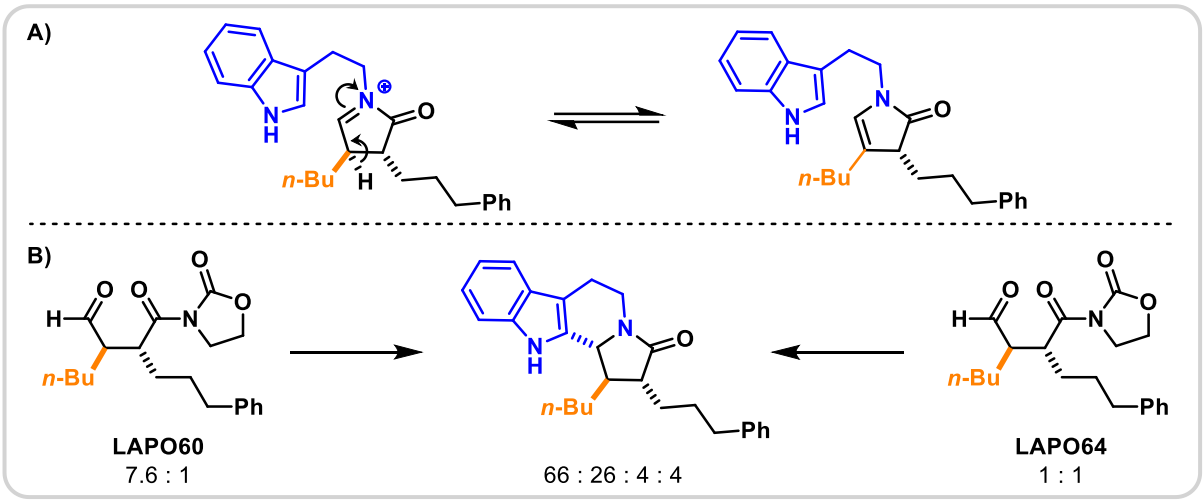

Figure 34: A) Possible epimerisation pathway in the reaction with tryptamine. B) Experimental support for epimerisation hypothesis.

Upon treatment with *para*-methoxy-benzylamine as a nucleophile (Figure 33, **B**), no second nucleophilic addition was detected, but rather a deprotonation in the β-position, resulting in the corresponding enamide (Figure 35), which can tautomerise to the more stabilised α,β-unsaturated amide (**13**). A similar reaction is assumed for 2-thienyl-methylamine (**15**) and 3,4-dimethoxyphenethylamine (**16**), evaluated by LCMS and crude NMR analysis. Due to the loss of valuable stereochemical information, this approach was not further investigated. When using quaternary 1,4-dicarbonyl substrates, that cannot be deprotonated in β-position, a γ-hydroxylation (**14**) was observed instead of polycycle formation, with a 3:1 d.r. on the newly formed chiral centre (Figure 33, **B**).

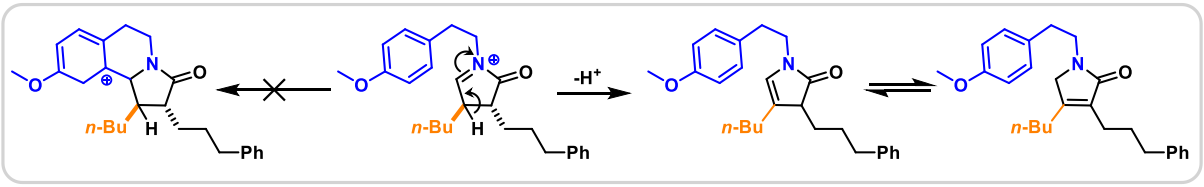

Figure 35: Proposed mechanism for the formation of α,β-unsaturated amide as a side product.

The presence of hydroxyl substituents on the aromatic nucleophile, as shown with serotonin and dopamine as reactants (Figure 33, **D**), had a detrimental effect on the transformation. No desired products cases were obtained in either case.

3.2.3 γ-substituted Lactone Synthesis

Following a procedure developed by a former member of the group (Alexander Beaton), a wide array of lactones can be obtained from 1,4-dicarbonyls. The reaction is performed using Grignard reagents in the presence of aluminium chloride. In the cyclisation process, a new chiral centre is formed in the γ-position. For *syn*-1,4-dicarbonyls, a wide range of Grignard nucleophiles showed a good stereoselectivity for the newly formed chiral centre (Figure 36).

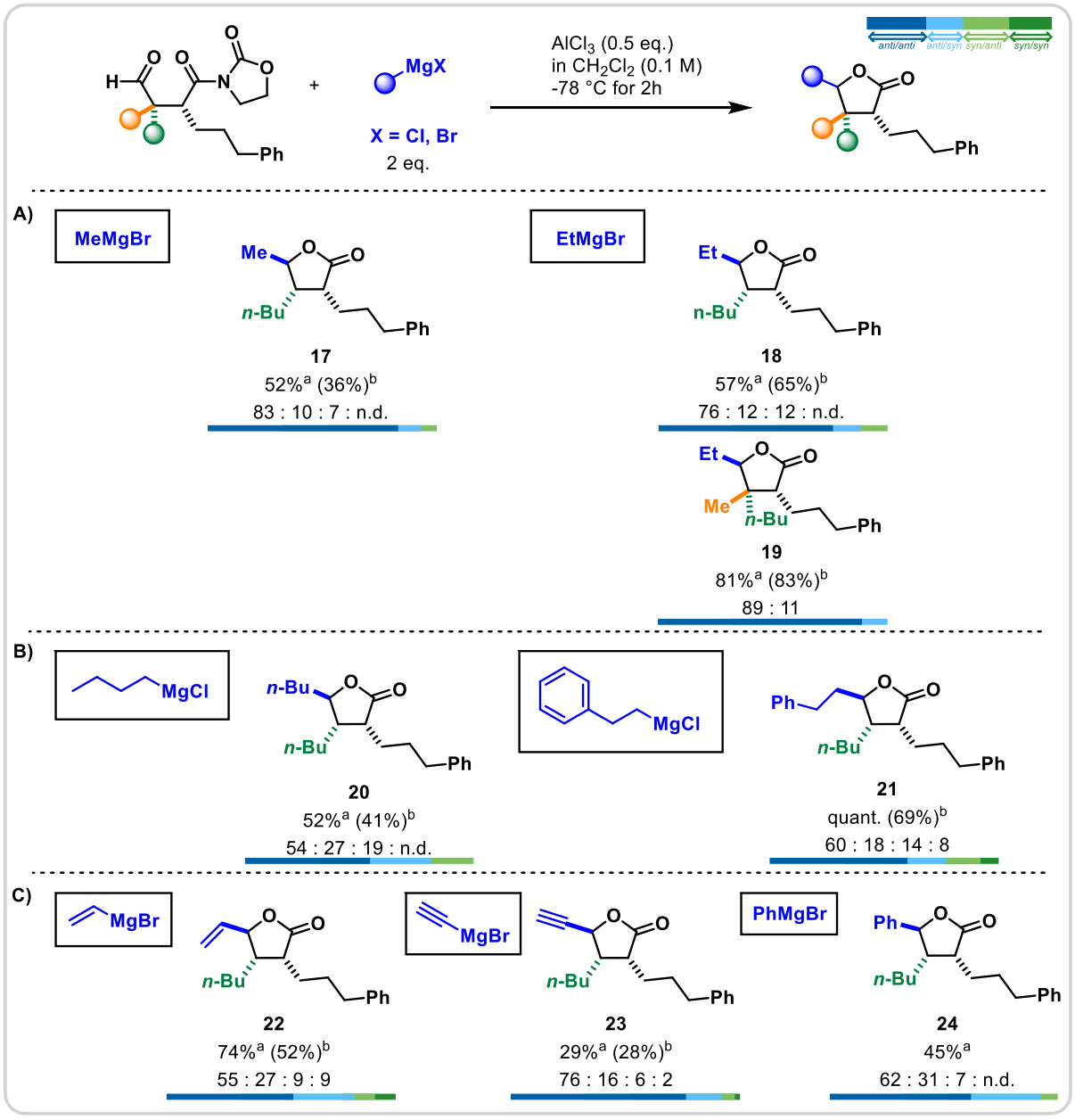

Figure 36: Scope of γ-substituted lactones via reaction of 1,4-dicarbonyls with RMgX. [a] NMR yield. [b] isolated yield.

Ethyl magnesium bromide was employed to probe the reaction and the desired lactone was obtained with excellent diastereomeric ratios (**18**,**19**). A similar selectivity was observed for methyl magnesium bromide (**17**) (Figure 36, **A**). More complex Grignard reagents resulted in a significant drop in selectivity as shown for longer alkyl chains (**20**) and phenethyl substituents (**21**) with 2:1 and 3:1 d.r. respectively (Figure 36, **B**). A similar trend is visible upon treatment of the 1,4-dicarbonyl with sp^2- and sp-hybridised Grignard reagents (Figure 36, **C**).

In the case of branched Grignard reagents, the desired cyclopentyl substituted lactone **25** was obtained only as a minor product whereas the γ-unsubstituted lactone **26** was observed in 28%. In this case, the Grignard reagent delivered a hydride for reduction rather than acting as an alkyl nucleophile. (Figure 37).

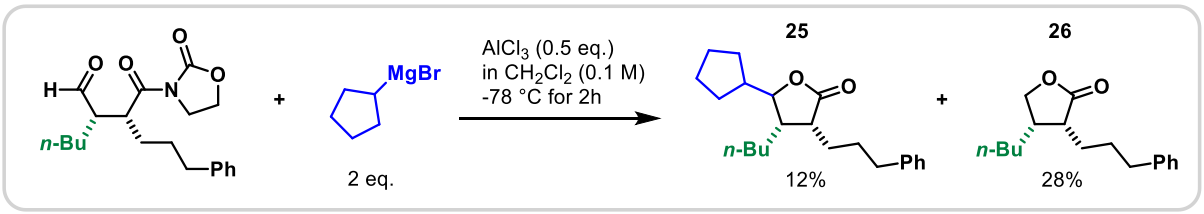

Figure 37: Cyclopentyl-Grignard reagents led to the reduced, γ-unsubstituted lactone as a major product

3.2.4 Hydrazine Nucleophiles

During the screening of potential bisnucleophiles (see section 3.2.2 Lactam Synthesis), substituted hydrazines were assessed under the same reaction conditions as for bisnucleophilic amines. The result was the formation of dihydropyridazinones **27** and **28** when methyl or phenylhydrazine were employed. However, hydrazine yielded the aromatised pyridazine derivative **29** as a sole product (Figure 38).

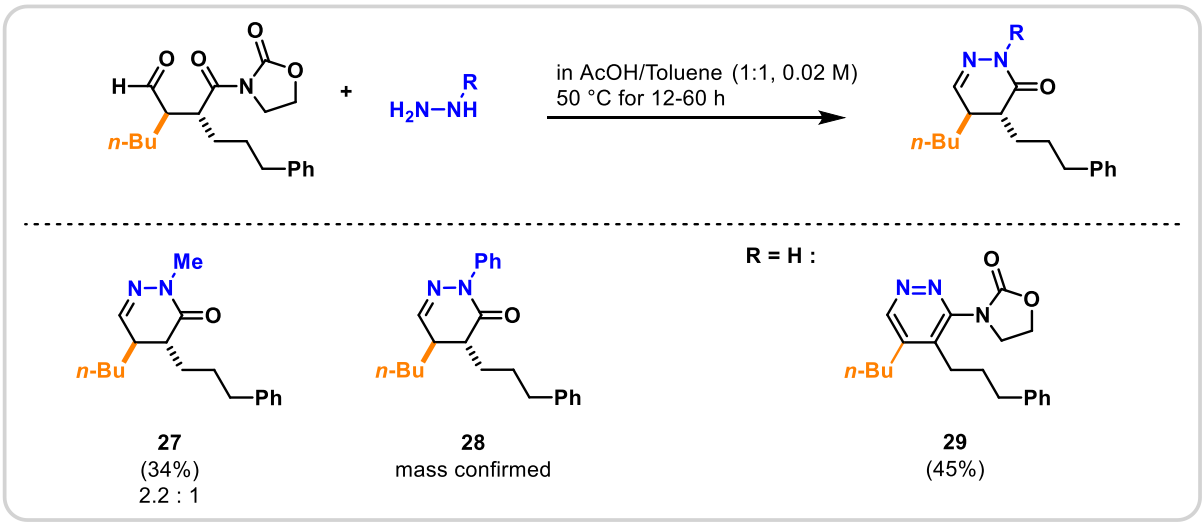

Figure 38: Scope of substrates with hydrazines as bisnucleophiles.

4. Conclusion

In this thesis, a recently published method for stereodivergent 1,4-dicarbonyl synthesis was investigated computationally to clarify unexpected reaction outcomes. Besides this computational study, the obtained 1,4-dicarbonyls were employed in diverse reactions aiming at obtaining valuable scaffolds.

A multitude of reaction pathways for the involved reactants were investigated to clarify the underlying reaction mechanism. Initial results showed the lowest energy geometries leading to opposite stereochemistry than the experiment. It was then proposed that the protonation event would be mediated by the sulfoxide itself. This hypothesis was reinforced by computational energy scans.

When comparing the different transition states for the sigmatropic rearrangement, qualitative results of the computational study match the experiment. Quantitative comparison shows a slight deviation of the experimental values, which nonetheless lies within the error margin of the highest achievable computational accuracy.

During the synthetic part of the thesis, I was able to prepare a wide range of γ-substituted lactone derivatives from organometallic Grignard reagents in the presence of Aluminium chloride, some of which with excellent diastereoselectivity on the newly formed chiral centre.

Attempted polycyclic lactam formation was limited to tryptamine as a bisnucleophile, with other investigated reactants resulting in a loss of both chiral centres. During the reaction with tryptamine, significant epimerisation was observed, influenced by the acid involved during the transformation.

Initial scans for hydrazine derivatives reacting with 1,4-dicarbonyls were performed, providing a diastereoselective synthesis pathway for trisubstituted dihydropyridazinone and pyridazine derivatives.

5. Experimental Section

All reactions were carried out in oven dried glassware with magnetic stirring. All solvents were used as received from commercial suppliers. All reagents were used as received from commercial suppliers unless otherwise stated. Neat infra-red spectra were recorded using a Perkin-Elmer Spectrum 100 FTIR spectrometer. Wavenumbers ($\tilde{\upsilon} = 1/\lambda$) are reported in cm−1. Mass spectra were obtained using a Finnigan MAT 8200 or (70 eV) or an Agilent 5973 (70 eV) spectrometer, using electrospray ionization (ESI). All 1 H-NMR and 13 C-NMR spectra were recorded using Bruker AV-400 or AV-600, spectrometers at 300 K. Chemical shifts (δ) are quoted in ppm and coupling constants (*J*) are quoted in Hz. The resonance of residual $CHCl_3$ in $CDCl_3$ (7.26 ppm for proton spectra and 77.16 ppm for carbon spectra) was used as internal references. 1 H NMR splitting patterns were designated as singlet (s), doublet (d), triplet (t) or combinations thereof, splitting patterns that could not be interpreted were designated as multiplet (m). Reactions were monitored by thin-layer chromatography (TLC) on Silica gel 60 F 254 aluminium plates (Merck). Chromatograms were visualized by fluorescence quenching with UV light at 254 nm or by staining using potassium permanganate. Flash column chromatography was performed using silica gel 60 (230– 400 mesh, Merck and co.).

Ynamide and vinylsulfoxide starting materials and quaternary 1,4-dicarbonyl compounds were supplied by co-workers.

General Procedure for 1,4-Dicarbonyl Synthesis

Ynamide (0.2 mmol, 2.0 equiv.), sulfoxide (0.1 mmol, 1.0 equiv.) and *i*-butanal (0.6 mmol, 6.0 equiv.) were dissolved in CH_2Cl_2 (1 mL) and H_2O (0.3 mmol, 3.0 equiv.) was added. To the 0° C mixture, 0.5 mL of a freshly prepared solution of Tf_2NH (0.035 mmol, 35 mol%) in CH_2Cl_2 was added to a vigorously stirred solution of all other reagents via syringe pump over 30 minutes. Reaction was allowed to stir for 2 h at 0 °C and then quenched by the addition of $NaHCO_3$ solution, extracted with CH_2Cl_2, dried over $MgSO_4$. Crude NMR was recorded with the internal standard mesitylene (1.0 equiv.). Final product was purified by column chromatography with EtOAc/Heptanes as specified for each compound.

anti-1,4-dicarbonyl: *(2R,3R)-2-butyl-3-(2-oxooxazolidine-3-carbonyl)-6-phenylhexanal*

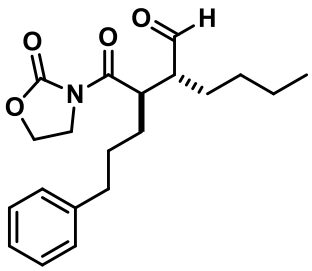

$C_{20}H_{27}NO_4$
MW: 345 g.mol^{-1}
Yield: 85% NMR,
72% isolated
d.r.: 8 : 1

The compound was obtained following the general 1,4-dicarbonyl procedure.

Spectral data matches literature.[39]

syn-1,4-dicarbonyl: *(2R,3S)-2-butyl-3-(2-oxooxazolidine-3-carbonyl)-6-phenylhexanal*

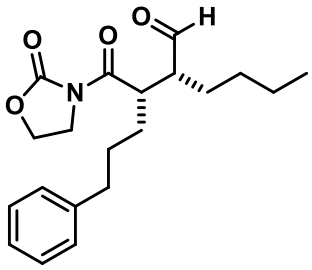

$C_{20}H_{27}NO_4$
MW: 345 g.mol^{-1}
Yield: 75% NMR,
68% isolated
d.r.: 8 : 1

The compound was obtained following the general 1,4-dicarbonyl procedure.

Spectral data matches literature.[39]

General Procedure A for γ-Lactam and Pyridazine Synthesis

To a stirred suspension of aldehyde (1.0 equiv.) in acetic acid and toluene solvent mixture (1:1, 0.02 M) was added bisnucleophile (3.0 equiv.). The mixture was heated to 50 °C for 12-60 h. After cooling to room temperature, the reaction mixture was washed with water and a saturated solution of sodium bicarbonate. The aqueous phase was extracted 3 times with CH_2Cl_2, dried over $MgSO_4$, filtered and the solvent was removed under reduced pressure. The crude was purified by automated flash chromatography (SiO_2, 5-30 % EtOAc in heptanes).

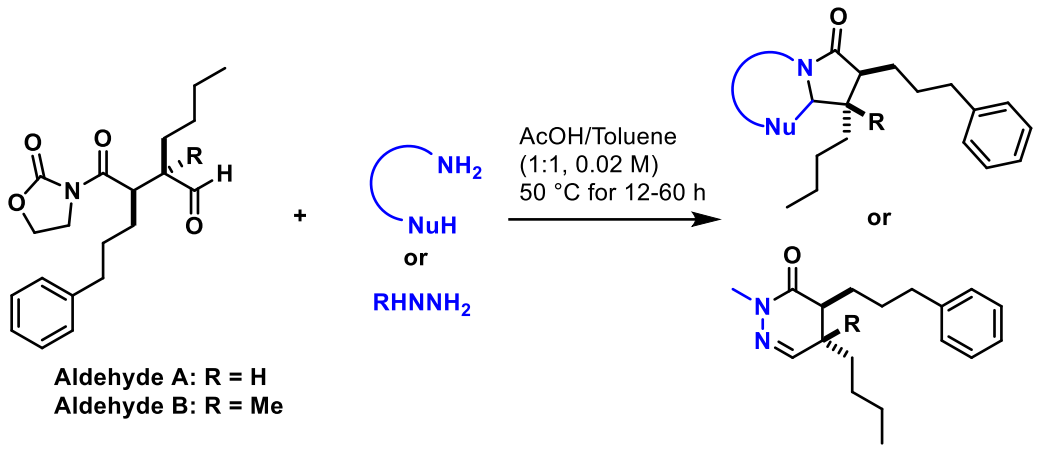

9: (±)-(3S,4S)-5-allyl-4-butyl-1-(4-methoxybenzyl)-3-(3-phenylpropyl)pyrrolidin-2-one

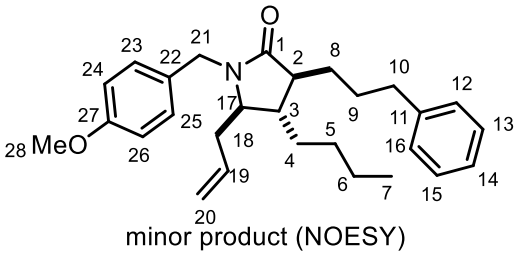

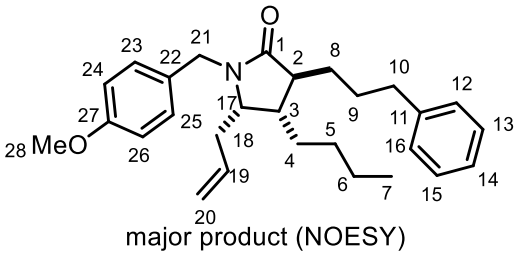

$C_{28}H_{37}NO_2$
MW: 420 g.mol^{-1}
Yield: 21% isolated
d.r.: SM: 7.6 : 1
crude: 51 : 41 : 8 : n.d.
isolated: 52 : 41 : 7 : n.d.

To a solution of aldehyde A (13.7 mg, 0.1 mmol, 1 equiv.) in CH_2Cl_2 (0.1 M) was added *p*-methoxy benzylamine (0.1 mmol, 1 equiv.) under an inert atmosphere. The mixture was

stirred for 3 h at room temperature and then cooled to -78 °C before $BF_3{\cdot}OEt_2$ (0.4 mmol, 4 equiv.) then allyl-TMS (0.2 mmol, 2 equiv.) were added.

The reaction was allowed to gradually warm to room temperature over the course of 16 h and then quenched with sat. aq. $NaHCO_3$, extracted with CH_2Cl_2, dried with $MgSO_4$, filtered and solvent removed under reduced pressure.

Final product was purified by automated flash chromatography (10 g cartridge, SiO_2 5-30 % EtOAc in heptanes) to afford the desired product as a yellow oil (8.6 mg, 21 %).

^{1}H NMR (600 MHz, $CDCl_3$): δ 7.28 (t, *J* = 7.6 Hz, 2H, H13+15), 7.21 – 7.17 (m, 3H, H12+14+16), 7.13 (dd, *J* = 13.8, 8.6 Hz, 2H, H23+25), 6.86 – 6.81 (m, 2H, H24+26), 5.69 (ddt, *J* = 17.1, 10.2, 7.1 Hz, 0.6H, $H19_{major}$), 5.57 (ddt, *J* = 17.2, 10.2, 7.1 Hz, 0.4H, $H19_{minor}$), 5.12 – 5.04 (m, 2H, H20), 5.04 – 4.93 (m, 1H, H21a), 3.86 (d, *J* = 11.1 Hz, 0.4H, $H21b_{minor}$), 3.83 (d, *J* = 11.0 Hz, 0.6H, $H21b_{major}$), 3.80 – 3.78 (m, 3H, H28), 3.41 (dd, *J* = 12.1, 6.0 Hz, 0.6H, $H17_{major}$), 3.02 (dt, *J* = 7.5, 3.9 Hz, 0.4H, $H17_{minor}$), 2.68 – 2.61 (m, 2H, H10), 2.37 – 2.20 (m, 2.6H, $H18+H2_{major}$), 2.16 – 2.11 (m, 0.4H, $H2_{minor}$), 1.94 – 1.86 (m, 0.6H, $H3_{major}$), 1.84 – 1.63 (m, 4.4H, $H8+9+3_{minor}$), 1.45 – 1.39 (m, 1H, H4a), 1.30 – 1.25 (m, 2H, H5), 1.23 – 1.12 (m, 3H, H4b+H6), 0.86 (t, *J* = 7.2 Hz, 1.8H, $H7_{major}$), 0.83 (t, *J* = 7.2 Hz, 1.2H, $H7_{minor}$).

^{13}C NMR (151 MHz, $CDCl_3$): δ 176.6 (C1), 158.92 ($C27_{minor}$), 158.89 ($C27_{major}$), 142.4 ($C11_{major}$), 142.2 ($C11_{minor}$), 134.4 ($C_{ar\ major}$), 133.1 ($C_{ar\ minor}$), 129.3 ($C_{ar\ minor}$), 129.2 ($C_{ar\ major}$), 128.9 (C_{ar}), 128.6(C_{ar}), 128.4 (C_{ar}), 128.27 (C_{ar}), 128.25 (C_{ar}), 125.71 (C_{ar}), 125.67 (C_{ar}), 118.7 ($C_{ar\ minor}$), 118.1 ($C_{ar\ major}$), 114.01 ($C11_{major}$), 113.98 ($C11_{minor}$), 60.6 ($C17_{minor}$), 56.6 ($C17_{major}$), 55.2 (C28), 48.1 ($C2_{minor}$), 46.1 ($C2_{major}$), 43.9 ($C21_{major}$), 43.5 ($C21_{minor}$), 42.0 ($C3_{major}$), 40.3 ($C3_{minor}$), 37.2 (C_{aliph}), 36.1 (C_{aliph}), 35.9 (C_{aliph}), 35.3 (C_{aliph}), 32.7 (C_{aliph}), 32.0 (C_{aliph}), 30.0 (C_{aliph}), 29.01 (C_{aliph}), 28.95 (C_{aliph}), 28.90 (C_{aliph}), 28.5 (C_{aliph}), 27.9 (C_{aliph}), 22.8 (C_{aliph}), 22.7 (C_{aliph}), 13.93 ($C7_{major}$), 13.90 ($C7_{minor}$).

HRMS (ESI$^+$): calculated for $C_{27}H_{32}N_2O$ $[M+H]^+$ m/z: 420.2897 found $[M+H]^+$ m/z: 420.2894

IR (neat cm^{-1})**:** 2927, 2857, 1771, 1682, 1512, 1245, 1034, 746, 700

***10**: (±)-1-butyl-2-(3-phenylpropyl)-1,2,5,6,11,11b-hexahydro-3H-indolizino[8,7-b]indol-3-one*

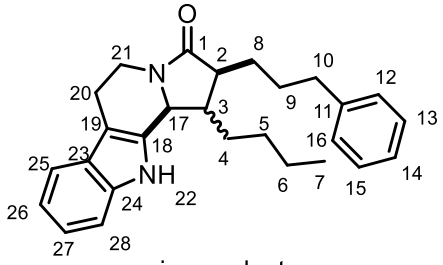

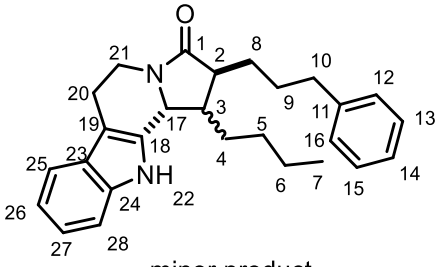

$C_{27}H_{32}N_2O$
MW: 400 g.mol^{-1}
Yield: 49% isolated
d.r.: SM: 7.6 : 1
crude: 66 : 26 : 4 : 4
isolated: 73 : 27 : n.d. : n.d.

The compound was obtained with a slight impurity following the general procedure A using aldehyde A (17.3 mg, 50 µmol, 1 equiv.) and tryptamine (24 mg, 150 µmol, 3 equiv.) with a reaction time of 60 h. The desired product was obtained as a colourless oil (9.8 mg, 49 %)

^{1}H NMR (700 MHz, $CDCl_3$): δ 7.86 (s, 0.3H, H22$_{minor}$), 7.77 (s, 0.7H, H22$_{major}$), 7.51 (d, *J* = 7.8 Hz, 0.3H, H25$_{minor}$), 7.48 (d, *J* = 7.8 Hz, 0.7H, H25$_{major}$), 7.36 (m, *J* = 8.1, 3.9 Hz, 1H, H28), 7.31 – 7.27 (m, 0.6H, H12$_{minor}$+16$_{minor}$), 7.22 – 7.17 (m, *J* = 7.6, 2.9, 1.5 Hz, 3.3H, H13$_{minor}$+14$_{minor}$+15$_{minor}$, H12$_{major}$+16$_{major}$, H27), 7.16 – 7.10 (m, 1.7H, H14$_{major}$+26), 7.07 (d, *J* = 7.0 Hz, 1.4H, H13+15$_{major}$), 5.02 (d, *J* = 6.2 Hz, 0.3H, H17$_{minor}$), 4.54 (dd, *J* = 13.2, 5.8 Hz, 0.7H, H21a$_{major}$) 4.53 – 4.51 (m, 0.7H, H17$_{major}$), 4.49 (dd, *J* = 12.9, 5.2 Hz, 0.3H, H21a$_{minor}$), 3.04 – 2.96 (m, 0.7H, H21b$_{major}$), 2.94 – 2.88 (m, 0.3H, H21b$_{minor}$), 2.88 – 2.81 (m, *J* = 11.5, 8.4, 5.2, 2.3 Hz, 1H, H20a), 2.80 – 2.74 (m, 1H, H20b), 2.72 (m, 0.3H, H10a$_{minor}$), 2.69 – 2.65 (m, 0.3H, H10b$_{minor}$), 2.61 – 2.52 (m, 1.4H, H10$_{major}$), 2.43 – 2.37 (m, 1H, H2), 2.30 – 2.24 (m, H3$_{minor}$), 2.06 – 2.00 (m, 0.7H, H3$_{major}$), 1.87 – 1.78 (m, 1H, H9a), 1.78 – 1.69 (m, *J* = 16.9, 12.1, 7.3, 2.5 Hz, 2H, H4), 1.68 – 1.56 (m, 3H, H8+H9b), 1.53 – 1.40 (m, 4H, H5+6), 0.98 (t, *J* = 8.0, 5.4 Hz, 2.1H, H7$_{major}$), 0.78 (t, 0.9H, H7$_{minor}$).

^{13}C NMR (176 MHz, $CDCl_3$): δ 175.4 (C1$_{minor}$), 174.7 (C1$_{major}$), 142.1 (C11$_{minor}$), 142.0 (C11$_{major}$), 136.4 (C24$_{minor}$), 136.2 (C24$_{major}$), 133.4 (C18$_{major}$), 130.3 (C18$_{minor}$), 128.5 (C13+15$_{minor}$), 128.4 (C12+16$_{minor}$), 128.3 (C13+15$_{major}$), 128.2 (C12+16$_{major}$), 126.9 (C23), 125.9 (C14$_{minor}$), 125.7 (C14$_{major}$), 122.3 (C27$_{major}$), 122.2 (C27$_{minor}$), 120.0 (C26$_{major}$), 119.8 (C26$_{minor}$), 118.5 (C25$_{major}$),

118.3 ($C25_{minor}$), 111.0 ($C28_{major}$), 110.9 ($C28_{minor}$), 110.6 ($C19_{minor}$), 108.9 ($C19_{major}$), 58.5 ($C17_{major}$), 56.7 ($C17_{minor}$), 49.4 ($C2_{minor}$), 48.3 ($C2_{major}$), 44.0 ($C3_{major}$), 42.0 ($C3_{minor}$), 37.8 ($C21_{major}$), 37.6 ($C21_{minor}$), 35.94 ($C10_{minor}$), 35.91 ($C10_{major}$), 34.9 (C20), 30.7 ($C_{aliph\ major}$), 29.88 ($C_{aliph\ minor}$), 29.86 ($C_{aliph\ minor}$), 29.7 ($C_{aliph\ major}$), 29.1 ($C_{aliph\ minor}$), 28.5 ($C_{aliph\ minor}$), 28.1 ($C_{aliph\ major}$), 23.1 ($C_{aliph\ major}$), 22.7 ($C_{aliph\ minor}$), 21.1 ($C_{aliph\ minor}$), 21.1 ($C_{aliph\ major}$), 14.07 ($C7_{minor}$), 14.05 ($C7_{major}$).

HRMS (ESI$^+$): calculated for $C_{27}H_{32}N_2O$ $[M+H]^+$ m/z: 401.2587 found $[M+H]^+$ m/z: 401.2583

IR (neat cm^{-1})**:** 2925, 1668, 1559

11: *(±)-1-butyl-2-(3-phenylpropyl)-1,2,5,6,11,11b-hexahydro-3H-indolizino[8,7-b]indol-3-one*

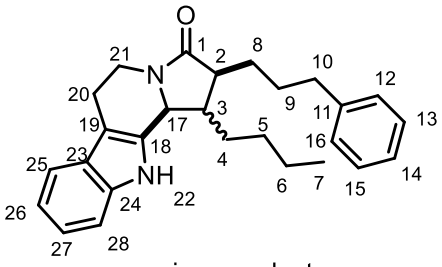

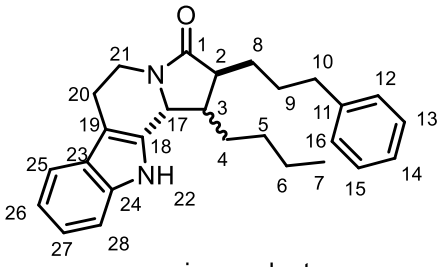

$C_{27}H_{32}N_2O$
MW: 401 $g.mol^{-1}$
Yield: 26% isolated
d.r.: SM: 7.5 : 1
crude: 56 : 20 : 17 : 7
isolated: 80 : 20 : n.d. : n.d.

The compounds could be obtained according to the general procedure A, with the exception of using only toluene as solvent (2 mL, 0.02 M) and trifluoroacetic acid (54 mg, 470 µmol, 9.4 equiv.). Aldehyde A (17.3 mg, 50 µmol, 1 equiv.) and tryptamine (24 mg, 150µmol, 3 equiv.) were reacted under the above conditions to form the desired product as a yellow oil (3.5 mg, 18 %)

Only major diastereomer characterised (see **10** for minor product)

^{1}H NMR (600 MHz, $CDCl_3$): δ 7.80 (s, 1H, H22), 7.51 (d, *J* = 7.8 Hz, 1H, H25), 7.36 (d, *J* = 8.1 Hz, 1H, H28), 7.31 – 7.28 (m, 2H, H12+16), 7.22 – 7.18 (m, 4H, H13+14+15+27), 7.16 – 7.12 (m, 1H, H26), 5.02 (d, *J* = 6.1 Hz, 1H, H17), 4.49 (dd, *J* = 12.8, 5.2 Hz, 1H, H21a), 2.94 – 2.88 (m, 1H, H21b), 2.85 (dd, *J* = 15.1, 4.4 Hz, 1H, H20a), 2.80 – 2.74 (m, 1H, H20b), 2.73 – 2.64 (m, 2H, H10), 2.40 – 2.36 (m, 1H, H2), 2.27 (app. ddd, *J* = 11.3, 6.2, 2.6 Hz, 1H, H3), 1.87 – 1.79 (m, 2H, H9), 1.76 – 1.69 (m, 1H, H4a), 1.64 – 1.59 (m, 2H, H8), 1.52 – 1.40 (m, 1H, H4b), 1.28 – 1.23 (m, 2H, H_{aliph}), 1.18 – 1.15 (m, 1H, H_{aliph}), 1.13 – 1.08 (m, 3H, H_{aliph}), 0.78 (t, *J* = 7.0 Hz, 3H, H7).

^{13}C NMR (151 MHz, $CDCl_3$): δ 175.3 (C1), 142.0 (C11), 136.4 (C24), 130.2 (C18), 128.5 (C13+15), 128.4 (C12+16), 126.9 (C23), 125.9 (C14), 122.2 (C27), 119.8 (C26), 118.3 (C25), 110.9 (C28), 56.6 (C17), 49.4 (C2), 42.0 (C3), 37.6 (C21), 35.9 (C10), 29.9 (C_{aliph}), 29.0 (C_{aliph}), 28.5 (C_{aliph}), 22.7 (C_{aliph}), 21.1 (C_{aliph}), 14.0 (C7).

HRMS (ESI$^+$): calculated for $C_{27}H_{32}N_2O$ $[M+H]^+$ m/z: 401.2587 found $[M+H]^+$ m/z: 401.2585

IR (neat cm^{-1})**:** 3271, 2927, 2857, 1664, 1436, 1264, 736, 700

12: *(±)-(1S,2S)-1-butyl-1-methyl-2-(3-phenylpropyl)-1,2,5,6,11,11b-hexahydro-3H-indolizino[8,7-b]indol-3-one*

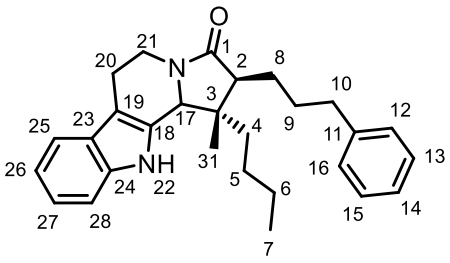

$C_{28}H_{34}N_2O$
MW: 415 $g.mol^{-1}$
Yield: 22% NMR,
19% isolated
d.r.: SM: 1 diastereomer
crude: 1 diastereomer
isolated: 1 diastereomer

The compound was obtained following the general procedure A using aldehyde B (18 mg, 50 µmol, 1 equiv.) and tryptamine (24 mg, 150 µmol, 3 equiv.) with a reaction time of 20 h as a yellow oil (4.0 mg, 19 %).

^{1}H NMR (700 MHz, $CDCl_3$): δ 7.73 (s, 1H, H22), 7.50 (d, *J* = 7.7 Hz, 1H, H25), 7.36 (d, *J* = 8.1 Hz, 1H, H28), 7.29 – 7.26 (m, 2H, H_{ar}), 7.22 – 7.16 (m, 4H, H_{ar}), 7.13 (t, *J* = 7.5, 1H, H14), 4.59 (s, 1H, H17), 4.54 – 4.50 (m, 1H, H21a), 2.88 – 2.83 (m, 2H, H21b+20a), 2.79 – 2.75 (m, 1H, H20b), 2.69 (t, *J* = 7.4 Hz, 2H, H10), 2.12 (dd, *J* = 11.0, 4.1 Hz, 1H, H2), 2.05 – 2.01 (m, 1H, 9a), 1.84 – 1.78 (m, 1H, H9b), 1.76 – 1.71 (m, 1H, H8a), 1.64 – 1.60 (m, 1H, H8b), 1.56 – 1.51 (m, 2H, H_{aliph}), 1.40 – 1.33 (m, 2H, H_{aliph}), 1.31 – 1.27 (m, 1H, H_{aliph}), 1.10 – 1.04 (m, 1H, H_{aliph}), 0.91 (t, *J* = 7.3 Hz, 3H, H7), 0.68 (s, 3H, H31).

^{13}C NMR (176 MHz, $CDCl_3$): δ 175.6 (C1), 142.0 (C11), 136.3 (C24), 130.1 (C18), 128.5 (C_{ar}), 128.27 (C_{ar}), 126.8 (C23), 125.7 (C14), 122.2 (C27), 119.9 (C26), 118.2 (C25), 111.0 (C28), 110.9

(C19), 61.9 (C17), 52.7 (C2), 44.8 (C3), 37.1 (C21), 35.7 (C10), 35.2 (C8), 28.6 (C_{aliph}), 26.6 (C_{aliph}), 26.4 (C_{aliph}), 23.4 (C_{aliph}), 21.2 (C31), 21.0 (C_{aliph}), 14.0 (C7).

IR (neat cm^{-1})**:** 3290,2955, 2928, 2859, 1663, 1450, 1425, 737, 699, 646

13: 4-butyl-1-(4-methoxybenzyl)-3-(3-phenylpropyl)-1,5-dihydro-2H-pyrrol-2-one

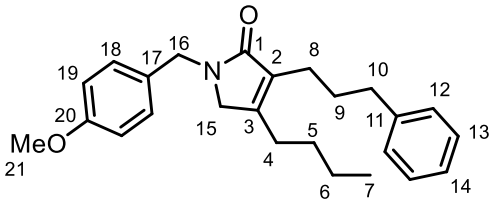

$C_{25}H_{31}NO_2$
MW: 377 $g.mol^{-1}$
Yield: 45% isolated

The reaction was conducted following the general procedure A using aldehyde A (8.8 mg, 25.5 µmol, 1 equiv.) and p-methoxy benzylamine (10.5 mg, 76.5 µmol, 3 equiv.) with a reaction time of 60 h.

Elimination product **13** was isolated as a yellow oil (4.3 mg, 45 %)

^{1}H NMR (600 MHz, $CDCl_3$): δ 7.27 (d, *J* = 7.7 Hz, 2H, H12), 7.20 (d, *J* = 7.2 Hz, 2H, H13), 7.18-7.15 (m, 3H, H14, H18), 6.85 (d, *J* = 8.6 Hz, 2H, H19), 4.54 (s, 2H, H16), 3.79 (s, 3H, H21), 3.60 (s, 2H, H15), 2.66 (t, 2H, H10), 2.32 (t, 2H, H8), 2.26 (t, 2H, H4), 1.85 (quint, 2H, H9), 1.36 (quint, 2H, H5), 1.29 (m, 2H, H6), 0.87 (t, *J* = 7.2 Hz, 3H, H7).

^{13}C NMR (151 MHz, $CDCl_3$): δ 172.4 (C1), 159.1 (C20), 150.8 (C3), 142.4 (C11), 132.5 (C2), 130.0 (C17), 129.5 (C18), 128.6 (C13), 128.4 (C12), 125.8 (C14), 114.2 (C19), 55.4 (C21), 52.0 (C15), 45.6 (C16), 36.0 (C10), 30.9 (C5), 30.4 (C9), 27.5 (C4), 23.8 (C8), 22.8 (C6), 13.9 (C7).

HRMS (ESI^+): calculated for $C_{25}H_{31}NO_2$ $[M+H]^+$ m/z: 378.2428 found $[M+H]^+$ m/z: 378.2428

IR (neat cm^{-1})**:** 2953, 2930, 2858, 1677, 1612, 1513, 1456, 1246, 1034, 745, 700

14: *(±)-(3S,4S)-4-butyl-5-hydroxy-1-(4-methoxybenzyl)-4-methyl-3-(3-phenylpropyl)pyrrolidin-2-one*

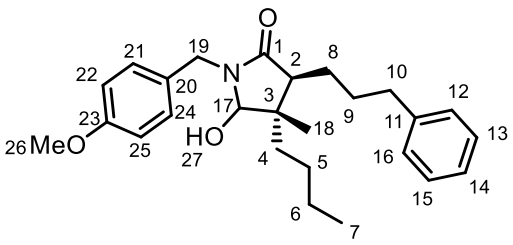

$C_{26}H_{35}NO_3$
MW: 410 g.mol^{-1}
Yield: 62% isolated
d.r.: SM: 1 diastereomer
crude: 70 : 24 : 5 : 1
isolated: 1 diastereomer

The reaction was conducted following the general procedure A using aldehyde B (8.8 mg, 25 µmol, 1 equiv.) and 4-methoxybenzylamine (10.3 mg, 75 µmol, 3 equiv.) with a reaction time of 60 h.

Compound **14** was isolated as a colourless oil (6.3 mg, 62 %)

^{1}H NMR (600 MHz, $CDCl_3$): δ 7.29 – 7.26 (m, 2H, H13+15), 7.22 – 7.15 (m, 5H, H12+16+21+24), 6.83 (d, *J* = 8.6 Hz, 2H, H22+25), 4.75 (d, *J* = 14.5 Hz, 1H, H19a), 4.54 (s, 1H, H17), 4.10 (d, *J* = 14.5 Hz, 1H, H19b), 3.78 (s, 3H, H26), 2.73 – 2.58 (m, 2H, H10), 2.35 (t, *J* = 6.6 Hz, 1H, H2), 2.07 – 1.97 (m, 1H, H9a), 1.87 (s, 1H, H, H27), 1.78 – 1.67 (m, 2H, H9b, H8a), 1.42 – 1.35 (m, 1H, H8b), 1.18 – 1.12 (m, 1H, H4a), 1.11 – 1.06 (m, 1H, H6a), 1.05 (s, 3H, H18), 1.04 – 1.01 (m, 1H, H6b), 1.01 – 0.97 (m, 1H, H4b), 0.97 – 0.91 (m, 1H, H5a), 0.81 – 0.75 (m, 1H, H5b), 0.72 (t, *J* = 7.3 Hz, 3H, H7).

^{13}C NMR (151 MHz, $CDCl_3$): δ 176.3 (C1), 159.2 (C23), 142.3 (C11), 130.0 (C13+15), 128.8 (C20), 128.4 (C12+16), 128.3 (C21+24), 125.7 (C14), 114.1 (C22+25), 85.6 (C17), 55.3 (C26), 49.6 (C2), 43.6 (C3), 43.5 (C19), 36.1 (C10), 34.1 (C4), 30.3 (C9), 26.2 (C5), 24.5 (C8), 23.3 (C6), 20.0 (C18), 13.8 (C7).

HRMS (ESI$^+$): calculated for $C_{26}H_{35}NO_3$ $[M+H]^+$ m/z: 410.2690 found $[M+H]^+$ m/z: 410.2687

IR (neat cm^{-1})**:** 3361, 2932, 2859, 1664, 1612, 1513, 1455, 1246, 1036, 745, 700

27: (±)-(4S,5S)-5-butyl-2-methyl-4-(3-phenylpropyl)-4,5-dihydropyridazin-3(2H)-one

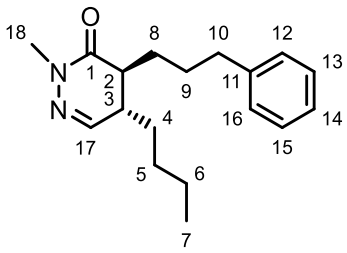

$C_{18}H_{26}N_2O$
MW: 286 g.mol^{-1}
Yield: 34% isolated
d.r.: SM: 7 : 1
isolated: 2.2 : 1 : n.d. : n.d.

The compound was obtained following the general procedure A using aldehyde A (8.8 mg, 25.5 µmol, 1 equiv.) and methylhydrazine (3.5 mg, 76.5 µmol, 3 equiv.) with a reaction time of 60 h. The desired product was obtained as a colourless oil (2.5 mg, 34 %)

^{1}H NMR (600 MHz, $CDCl_3$): δ 7.28 – 7.26 (m, 2H, H12+16), 7.19 – 7.14 (m, 3H, H13-15), 7.05 (t, *J* = 2.8 Hz, 1H, H17), 3.33 (s, 3H, H18), 2.62 (dd, *J* = 15.5, 7.5 Hz, 2H, H10), 2.56 (ddd, *J* = 9.3, 6.3, 3.1 Hz, 0.3H, $H3_{syn}$), 2.44 (dd, *J* = 13.7, 6.5 Hz, 0.3H, $H2_{syn}$), 2.37 – 2.29 (m, 0.7+0.7H, $H2+3_{anti}$), 1.70 – 1.63 (m, 2H, H8), 1.53 – 1.44 (m, 2H, H9), 1.42 – 1.33 (m, 2H, H4), 1.32 – 1.28 (m, 4H, H5-6), 0.88 (t, *J* = 6.9 Hz, 3H, H7).

^{13}C NMR (151 MHz, $CDCl_3$): δ 168.1 (C1), 149.5 ($C17_{syn}$), 147.6 ($C17_{anti}$), 141.8 (C11), 128.39 (C13+15), 128.35 ($C12+16_{anti}$), 128.32 ($C12+16_{syn}$), 125.9 ($C14_{anti}$), 125.8 ($C14_{syn}$), 42.2 ($C2_{anti}$), 40.1 ($C2_{syn}$), 38.8 ($C3_{anti}$), 37.0 ($C3_{syn}$), 36.3 ($C18_{anti}$), 36.1 ($C18_{syn}$), 35.70 ($C10_{syn}$), 35.67 ($C10_{anti}$), 30.2 ($C8_{anti}$), 29.7 ($C9_{anti}$), 29.1 ($C9_{syn}$), 28.8 ($C8_{syn}$), 28.7 ($C5_{anti}$), 28.4 ($C4_{anti}$), 26.1 ($C5_{syn}$), 24.2 ($C4_{syn}$), 22.64 ($C6_{anti}$), 22.62 ($C6_{syn}$), 13.8 (C7).

HRMS (ESI$^+$): calculated for $C_{18}H_{26}N_2O$ $[M+H]^+$ m/z: 287.2118 found $[M+H]^+$ m/z: 287.2118

IR (neat cm^{-1})**:** 2929, 2857, 1769, 1671, 1267, 741, 702

29: *3-(5-butyl-4-(3-phenylpropyl)pyridazin-3-yl)oxazolidin-2-one*

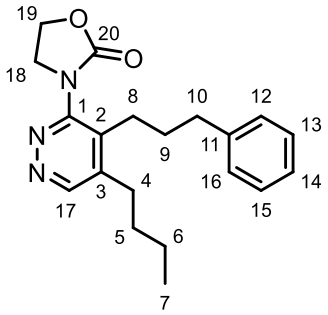

$C_{20}H_{25}N_3O_2$
MW: 339 g.mol^{-1}
Yield: 45% isolated

The reaction was conducted following the general procedure A using aldehyde A (8.8 mg, 25.5 µmol, 1 equiv.) and hydrazine monochloride (5.2 mg, 76.5 µmol, 3 equiv.) with a reaction time of 60 h.

The aromatic compound **29** was isolated as a colourless oil (3.9 mg, 45 %)

^{1}H NMR (600 MHz, $CDCl_3$): δ 8.83 (s, 1H, H17), 7.31 (t, *J* = 7.5 Hz, 2H, H13+15), 7.22 (t, *J* = 7.4 Hz, 1H, H14), 7.17 (d, *J* = 7.3 Hz, 2H, H12+16), 4.47 (t, *J* = 7.8 Hz, 2H, H19), 4.27 (t, *J* = 7.7 Hz, 2H, H18), 2.77 (t, 2H, H8), 2.68 (t, *J* = 7.1 Hz, 2H, H10), 2.55 (t, 2H, H4), 1.80 (quint, 2H, H9), 1.54 (quint, 2H, H5), 1.35 (dq, *J* = 14.7, 7.4 Hz, 2H, H6), 0.93 (t, *J* = 7.3 Hz, 3H, H7).

^{13}C NMR (151 MHz, $CDCl_3$): δ 156.3 (C1), 154.2 (C20), 152.0 (C17), 142.8 (C3), 141.1 (C11), 137.7 (C2), 128.5 (C13+15), 128.4 (C12+16), 126.2 (C14), 63.1 (C19), 46.7 (C18), 35.8 (C10), 32.2 (C5), 31.0 (C9), 29.5 (C4), 26.0 (C8), 22.6 (C6), 13.7 (C7).

HRMS (ESI$^+$): calculated for $C_{20}H_{25}N_3O_2$ $[M+H]^+$ m/z: 340.2020 found $[M+H]^+$ m/z: 340.2018

General Procedure B for Trisubstituted γ-Lactone Synthesis

To a mixture of aldehyde (1.0 equiv.) and $AlCl_3$ (0.50 equiv.) in CH_2Cl_2 (0.1 M) at -78 °C was added Grignard reagent (2.0 equiv.) under an inert atmosphere. The mixture was stirred for 2 h at room temperature. The reaction was quenched with sat. aq. NH_4Cl solution, extracted with CH_2Cl_2, dried over $MgSO_4$, filtered and the solvent was removed under reduced pressure. Crude NMR was recorded with the internal standard mesitylene (1.0 equiv.). Final product was purified by automated flash chromatography (SiO_2, 0-25 % EtOAc in heptanes).

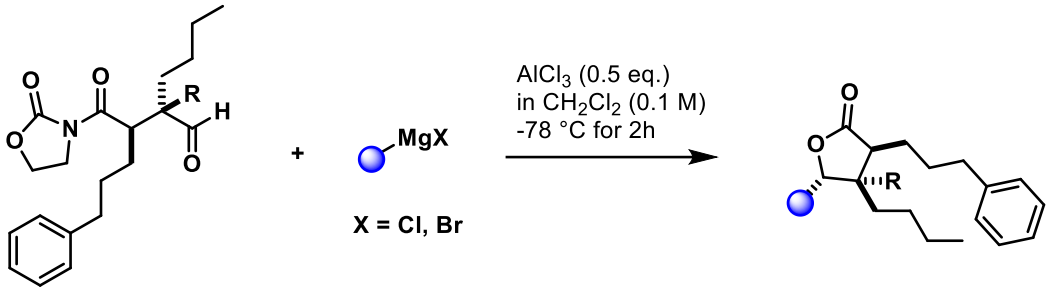

17: (±)-(3S,4R,5S)-4-butyl-5-methyl-3-(3-phenylpropyl)dihydrofuran-2(3H)-one

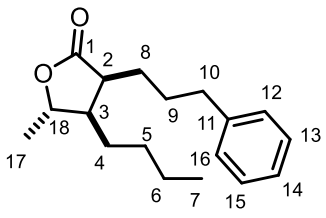

$C_{18}H_{26}O_2$
MW: 274 g.mol^{-1}
Yield: 52% NMR,
36% isolated
d.r.: SM d.r.: 6.4 : 1
crude: 83 : 10 : 7 : n.d.
isolated: 81 : 9 : 6 : 4

The compound was obtained following the general procedure B using aldehyde C (19.1 mg, 55 µmol, 1 equiv.) and methyl magnesium bromide (37 µL of a 3 M Solution in Et_2O, 110 µmol, 2 equiv.) as a colourless oil (5.5 mg, 36 %)

Only major diastereomer characterised.

^{1}H NMR (600 MHz, $CDCl_3$): δ 7.29 – 7.26 (m, 2H, H13+15), 7.20 – 7.16 (m, 3H, H12+14+16), 4.28 (app. p, *J* = 6.3 Hz, 1H, H18), 2.67 (t, *J* = 7.4 Hz, 2H, H10), 2.62 (app. dd, *J* = 15.1, 7.7 Hz, 1H, H2), 2.06 – 2.01 (m, 1H, H3), 1.91 – 1.83 (m, 1H, H8a), 1.74 – 1.61 (m, 2H, H8b, H9a), 1.55

– 1.49 (m, 1H, H9b), 1.34 (d, *J* = 6.3 Hz, 3H, H17), 1.32 – 1.30 (m, 1H, H4a), 1.29 – 1.27 (m, 2H, H6), 1.26 – 1.25 (m, 1H, H5a), 1.24 – 1.18 (m, 2H, H4b+H5b), 0.90 – 0.86 (m, 3H, H7).

^{13}C NMR (151 MHz, $CDCl_3$): δ 178.5 (C1), 141.7 (C11), 128.4 (C13+15), 128.3 (C12+16), 125.9 (C14), 79.2 (C18), 45.5 (C3), 42.1 (C2), 35.7 (C10), 29.5 (C5), 28.9 (C8), 26.4 (C4), 24.4 (C9), 22.7 (C6), 19.7 (C17), 13.9 (C7).

HRMS (ESI^+): calculated for $C_{18}H_{26}O_2$ $[M+H]^+$ m/z: 275.2006 found $[M+H]^+$ m/z: 275.2004

IR (neat cm^{-1})**:** 2930, 2860, 1768, 1603, 1454, 1188, 746, 700

18: (±)-(3S,4R,5S)-4-butyl-5-ethyl-3-(3-phenylpropyl)dihydrofuran-2(3H)-one

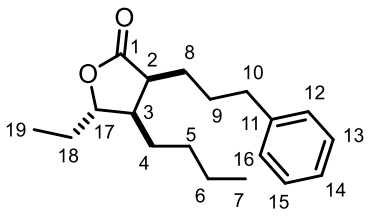

$C_{19}H_{28}O_2$
MW: 288 $g.mol^{-1}$
Yield: 57% NMR,
65% isolated
d.r.: SM: 8.5 : 1
crude: 76 : 12 : 12 : n.d.
isolated: 76 : 11 : 9 : 4

The compound was obtained following the general procedure B using aldehyde C (19.1 mg, 55 µmol, 1 equiv.) and ethyl magnesium bromide (37 µL of a 3 M Solution in Et_2O, 110 µmol, 2 equiv.) as a colourless oil (10.3 mg, 65 %)

Only major diastereomer characterised.

^{1}H NMR (400 MHz, $CDCl_3$): δ 7.23 – 7.20 (m, 2H, H_{ar}), 7.13 – 7.09 (m, 3H, H_{ar}), 4.00 (dd, *J* = 11.1, 6.5 Hz, 1H, H17), 2.60 (t, *J* = 6.3 Hz, 2H, H10), 2.53 (app. dd, *J* = 15.0, 7.7 Hz, 1H, H2), 2.07 – 1.98 (m, 1H, H3), 1.81 – 1.75 (m, 1H, H8a), 1.66 – 1.60 (m, 2H, H8b+9a), 1.59 – 1.50 (m, 2H, H18), 1.46 – 1.39 (m, 1H, H9b), 1.23 – 1.09 (m, 6H, H_{aliph}), 0.93 (t, *J* = 7.4 Hz, 3H, H19), 0.83 – 0.79 (m, 3H, H7).

^{13}C NMR (151 MHz, $CDCl_3$): δ 128.41 (C_{ar}), 128.38 (C_{ar}), 125.9 (C_{ar}), 84.4 (C17), 42.8 (C3), 42.0 (C2), 35.7 (C10), 29.4 (C_{aliph}), 29.1 (C_{aliph}), 27.0 (C_{aliph}), 26.7 (C_{aliph}), 24.5 (C_{aliph}), 22.7 (C_{aliph}), 13.9 (C_{aliph}), 10.1 (C_{aliph}). Quarternary carbons not detected due to low concentration.

HRMS (ESI$^+$): calculated for $C_{19}H_{28}O_2$ [M+H]$^+$ m/z: 289.2162 found [M+H]$^+$ m/z: 289.2162

IR (neat cm^{-1})**:** 2931, 2860, 1768, 1455, 1186, 967, 746, 700

19: (±)-(3S,4R,5S)-4-butyl-5-ethyl-4-methyl-3-(3-phenylpropyl)dihydrofuran-2(3H)-one

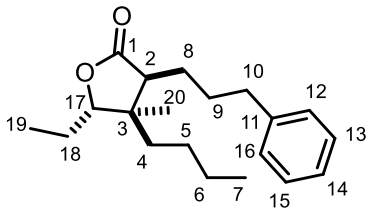

$C_{20}H_{30}O_2$
MW: 302 g.mol^{-1}
Yield: 81% NMR,
83% isolated
d.r.: SM 1 diastereomer
crude: 89 : 11
isolated: 91 : 9

The compound was obtained following the general procedure B using aldehyde D (18 mg, 50 µmol, 1 equiv.) and ethyl magnesium bromide (33 µL of a 3 M Solution in THF, 100 µmol, 2 equiv.). The desired product was obtained as a colourless oil (12.5 mg, 83 %)

^{1}H NMR (700 MHz, $CDCl_3$): δ 7.31 – 7.26 (m, 2H, H13+15), 7.20 – 7.15 (m, 3H, H12+14+16), 4.02 (dd, *J* = 7.2, 6.4 Hz, 1H, H17), 2.69 – 2.64 (m, 2H, H10), 2.20 (dd, *J* = 9.8, 4.9 Hz, 1H, H2), 2.04 – 1.99 (m, 1H, H8a), 1.75 – 1.70 (m, 1H, H8b), 1.64 – 1.59 (m, 1H, H9a), 1.53 – 1.49 (m, 2H, H18), 1.49 – 1.44 (m, 1H, H9b), 1.27 – 1.21 (m, 4H, H4+6), 1.15 – 1.08 (m, 2H, H5), 1.06 – 1.03 (m, 3H, H19), 0.98 (s, 3H, H20), 0.87 (t, *J* = 7.1 Hz, 3H, H7).

^{13}C NMR (176 MHz, $CDCl_3$): δ 178.7 (C1), 141.8 (C11), 128.4 (C13+15), 128.3 (C12+16), 125.8 (C14), 86.9 (C17), 49.6 (C2), 44.3 (C3), 35.7 (C10), 34.1 (C4), 29.2 (C8), 26.4 (C6), 24.6 (C9), 23.3 (C5), 23.0 (C18), 20.3 (C20), 13.9 (C7), 11.2 (C19).

HRMS (ESI$^+$): calculated for $C_{20}H_{30}O_2$ [M+H]$^+$ m/z: 303.2319 found [M+H]$^+$ m/z: 303.2317

IR (neat cm^{-1})**:** 2956, 2933, 2861, 1768, 1462, 970, 744, 700

20: *(±)- (3S,4R)-4,5-dibutyl-3-(3-phenylpropyl)dihydrofuran-2(3H)-one*

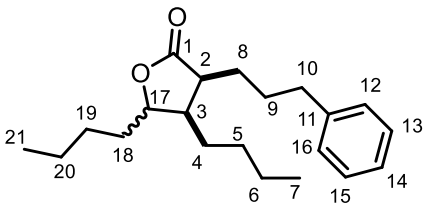

$C_{21}H_{32}O_2$
MW: 316 g.mol^{-1}
Yield: 52% NMR,
41% isolated
d.r.: SM: 3.1 : 1
crude: 54 : 27 : 19 : n.d.
isolated: 41 : 33 : 15 : 11

The compound was obtained following the general procedure B using aldehyde C (17.3 mg, 50 µmol, 1 equiv.) and *n*-butyl magnesium chloride (58 µL of a 20% Solution in THF/Toluene, 100 µmol, 2 equiv.). The desired product was isolated as a colourless oil (6.5 mg, 41 %).

Only major diastereomer characterised.

^{1}H NMR (600 MHz, $CDCl_3$): δ 7.29 – 7.26 (m, 2H, H13+15), 7.20 – 7.17 (m, 3H, H12+14+16), 4.12 (dt, *J* = 7.6, 5.0 Hz, 1H, H17), 2.69 – 2.64 (m, 2H, H10), 2.60 (app. dd, *J* = 15.1, 7.7 Hz, 1H, H2), 2.10 – 2.05 (m, 1H, H3), 1.87 – 1.82 (m, 1H, H, H8a), 1.72 – 1.67 (m, 2H, H8b+9a), 1.60 – 1.55 (m, 2H, H18), 1.52 – 1.43 (m, 2H, H9b+H_{aliph}), 1.37 – 1.23 (m, 7H, H_{aliph})), 1.22 – 1.16 (m, 2H, H_{aliph})), 0.92 – 0.87 (m, 6H, H7+21).

^{13}C NMR (151 MHz, $CDCl_3$): δ 178.6 (C1), 141.8 (C11), 128.39 (C13+15), 128.35 (C12+16), 125.9 (C14), 83.1 (C17), 43.3 (C3), 42.0 (C2), 35.7 (C10), 33.7 (C18), 29.4 (C_{aliph}), 29.1 (C_{aliph}), 27.9 (C_{aliph}), 26.7 (C_{aliph}), 24.5 (C_{aliph}), 22.7 (C_{aliph}), 22.5 (C_{aliph}), 13.9 (C7+21).

HRMS (ESI$^+$): calculated for $C_{21}H_{32}O_2$ $[M+H]^+$ m/z: 317.2475 found $[M+H]^+$ m/z: 317.2476

IR (neat cm^{-1})**:** 2954, 2930, 2860, 1767, 1455, 1183, 746, 700

21: *(±)-(3S,4R)-4-butyl-5-phenethyl-3-(3-phenylpropyl)dihydrofuran-2(3H)-one*

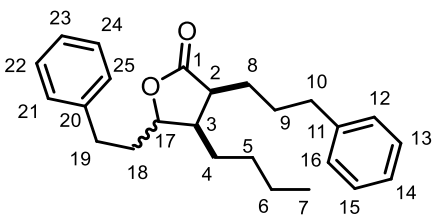

$C_{25}H_{32}O_2$
MW: 365 g.mol^{-1}
Yield: quant. NMR,
69% isolated
d.r.: SM: 3.1 : 1
crude: 49 : 40 : 9 : 2
isolated: 37 : 36 : 16 : 11

The compound was obtained following the general procedure B using aldehyde C (17.3 mg, 50 µmol, 1 equiv.) and phenethyl magnesium chloride (100 µL of a 1 M Solution in THF/Toluene, 100 µmol, 2 equiv.). The desired product was isolated as a colourless oil (12.6 mg, 69 %).

^{1}H NMR (600 MHz, $CDCl_3$): δ 7.31 – 7.27 (m, 4H, H_{ar}), 7.20 – 7.17 (m, 6H, H_{ar}), 4.14 (dd, *J* = 12.8, 5.3 Hz, 1H, H17), 2.87 – 2.81 (m, 1H, H19a), 2.69 – 2.60 (m, 4H, H19b+3+10), 2.13 – 2.08 (m, 1H, H2), 1.93 – 1.85 (m, 3H, H8a+9), 1.72 – 1.66 (m, 2H, H8b+H18a), 1.53 – 1.47 (m, 1H, H18b), 1.32 – 1.25 (m, 3H, H_{aliph}), 1.22 – 1.15 (m, 3H, H_{aliph}), 0.86 (t, *J* = 7.1 Hz, 3H, H7).

^{13}C NMR (151 MHz, $CDCl_3$): δ 178.5 (C1), 141.7 (C11), 140.9 (C20), 128.5 (C_{ar}), 128.39 (C_{ar}), 128.38 (C_{ar}), 128.36 (C_{ar}), 126.1 (C_{ar}), 125.9 (C_{ar}), 82.2 (C17), 43.5 (C2), 42.1 (C3), 36.0 (C_{aliph}), 35.7 (C_{aliph}), 32.1 (C_{aliph}), 29.4 (C_{aliph}), 29.0 (C_{aliph}), 26.6 (C_{aliph}), 24.5 (C_{aliph}), 22.7 (C_{aliph}), 13.9 (C7).

HRMS (ESI^+): calculated for $C_{25}H_{32}O_2$ $[M+H]^+$ m/z: 365.2476 found $[M+H]^+$ m/z: 365.2475

IR (neat cm^{-1})**:** 3026, 2929, 2860, 1769, 1496, 1454, 747, 699

Second diastereomer:

^{1}H NMR (600 MHz, $CDCl_3$): δ 7.32 – 7.26 (m, 4H, H_{ar}), 7.23 – 7.16 (m, 6H, H_{ar}), 4.34 – 4.27 (m, 1H, H17), 2.91 (ddd, *J* = 14.1, 9.5, 5.0 Hz, 1H, H19a), 2.73 – 2.66 (m, 2H, H19b+H10a), 2.66 – 2.59 (m, 1H, H10b), 2.55 (dd, *J* = 14.8, 7.5 Hz, 1H, H3), 2.42 – 2.36 (m, 1H, H2), 2.05 – 1.98 (m, 1H, H18a), 1.90 – 1.83 (m, 2H, H18b+H8a), 1.82 – 1.76 (m, 1H, H9a), 1.72 – 1.66 (m, 1H, H8b), 1.53 – 1.48 (m, 1H, H9b), 1.33 – 1.27 (m, 2H, H_{aliph}), 1.25 – 1.16 (m, 4H, H_{aliph}), 0.85 (t, *J* = 6.9 Hz, 3H, H7).

^{13}C NMR (151 MHz, $CDCl_3$): δ 178.7 (C1), 141.8 (C11), 141.0 (C20), 128.5 (C_{ar}), 128.39 (C_{ar}), 128.36 (C_{ar}), 126.2 (C_{ar}), 125.9 (C_{ar}), 81.6 (C17), 45.1 (C2), 41.5 (C3), 35.7 (C_{aliph}), 32.53 (C_{aliph}), 32.51 (C_{aliph}), 29.8 (C_{aliph}), 29.7 (C_{aliph}), 25.2 (C_{aliph}), 23.8 (C_{aliph}), 23.2 (C_{aliph}), 13.8 (C7). 1 aromatic carbon missing, peak intensity suggests overlap at 128.5

HRMS (ESI^+): calculated for $C_{25}H_{32}O_2$ $[M+H]^+$ m/z: 365.2476 found $[M+H]^+$ m/z: 365.2472

IR (neat cm^{-1})**:** 3026, 2953, 2931, 2860, 1769, 1603, 1496, 1454, 747, 700

22: (±)-(3S,4R,5S)-4-butyl-3-(3-phenylpropyl)-5-vinyldihydrofuran-2(3H)-one

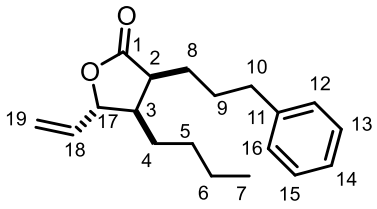

$C_{19}H_{26}O_2$
MW: 286 $g.mol^{-1}$
Yield: 74% NMR,
52% isolated
d.r.: SM: 8.5 : 1
crude: 55 : 27 : 9 : 9
isolated: 58 : 31 : 7 : 4

The compound was obtained following the general procedure B using aldehyde C (17.3 mg, 50 µmol, 1 equiv.) and vinyl magnesium bromide (100 µL of a 1 M Solution in THF/Toluene, 100 µmol, 2 equiv.) as a yellow oil (7.4 mg, 52 % yield)

^{1}H NMR (600 MHz, $CDCl_3$): δ 7.29 – 7.26 (m, 2H, H_{ar}), 7.20 – 7.17 (m, 3H, H_{ar}), 5.81 (ddd, *J* = 16.7, 10.5, 5.8 Hz, 1H, H18), 5.34 (d, *J* = 17.1 Hz, 1H, H19a), 5.25 (d, *J* = 10.5 Hz, 1H, H19b), 4.58 (t, *J* = 5.3 Hz, 1H, H17), 2.66 (t, *J* = 6.3 Hz, 2H, H10), 2.60 (app. dd, *J* = 15.0, 7.5 Hz, 1H, H2), 2.20 – 2.14 (m, 1H, H3), 1.89 – 1.81 (m, 1H, H8a), 1.71 – 1.66 (m, 2H, H9), 1.53 – 1.49 (m, 1H, H8b), 1.35 – 1.26 (m, 4H, H_{aliph}), 1.24 – 1.18 (m, 2H, H_{aliph}), 0.88 (t, *J* = 6.9 Hz, 3H, H7).

^{13}C NMR (151 MHz, $CDCl_3$): δ 178.3 (C1), 141.7 (C11), 135.1 (C18), 128.38 (C_{ar}), 128.36 (C_{ar}), 125.9 (C_{ar}), 117.6 C(19), 82.6 (C17), 44.1 (C3), 41.5 (C2), 35.6 (C_{aliph}), 29.3 (C_{aliph}), 29.0 (C_{aliph}), 26.1 (C_{aliph}), 24.3 (C_{aliph}), 22.6 (C_{aliph}), 13.9 (C7).

HRMS (ESI$^+$): calculated for $C_{19}H_{26}O_2$ $[M+Na]^+$ m/z: 309.1825 found $[M+Na]^+$ m/z: 309.1825

IR (neat cm^{-1})**:** 2953, 2930, 2860, 1773, 744, 700

23: (±)-(3S,4R,5R)-4-butyl-5-ethynyl-3-(3-phenylpropyl)dihydrofuran-2(3H)-one

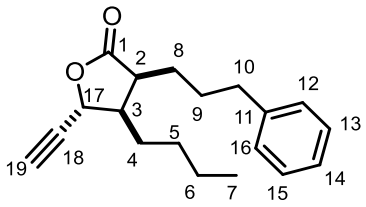

$C_{19}H_{24}O_2$
MW: 284 $g.mol^{-1}$
Yield: 29% NMR,
28% isolated
d.r.: SM: 8.5 : 1
crude: 8 : 1 : n.d. : n.d.
isolated: 1 diastereomer

The compound was obtained following the general procedure B using aldehyde C (17.3 mg, 50 µmol, 1 equiv.) and ethynyl magnesium bromide (200 µL of a 0.5 M Solution in THF/Toluene, 100 µmol, 2 equiv.). The desired product was isolated as a colourless oil (4.0 mg, 28 %).

^{1}H NMR (700 MHz, $CDCl_3$): δ 7.28 (t, *J* = 7.6 Hz, 2H, H_{ar}), 7.20 – 7.17 (m, 3H, H_{ar}), 4.80 – 4.77 (m, 1H, H17), 2.83 (dd, *J* = 15.1, 7.4 Hz, 1H, H2), 2.73 – 2.61 (m, 3H, H10), 2.58 (d, *J* = 2.1 Hz, 1H, H19), 2.51 – 2.47 (m, 1H, H3), 1.89 – 1.83 (m, 1H, H8a), 1.76 – 1.72 (m, 1H, H9a), 1.70 – 1.67 (m, 1H, H8b), 1.50 – 1.46 (m, 1H, H9b), 1.36 – 1.33 (m, 2H, H_{aliph}), 1.30 – 1.26 (m, 2H, H_{aliph}), 1.25 – 1.18 (m, 2H, H_{aliph}), 0.89 (t, *J* = 6.9 Hz, 3H, H7).

^{13}C NMR (176 MHz, $CDCl_3$): δ 177.3 (C1), 141.6 (C11), 128.40 (C_{ar}), 128.37 (C_{ar}), 126.0 (C_{ar}), 75.5 (C18), 70.5 (C17), 45.9 (C3), 42.0 (C2), 35.6 (C_{aliph}), 29.1 (C_{aliph}), 29.1 (C_{aliph}), 26.2 (C_{aliph}), 24.3 (C_{aliph}), 22.5 (C_{aliph}), 13.9 (C7). C19 missing.

HRMS (ESI$^+$): calculated for $C_{19}H_{24}O_2$ $[M+ Na]^+$ m/z: 307.1669 found $[M+ Na]^+$ m/z: 307.1668

25: (±)-(3S,4R,5S)-4-butyl-5-cyclopentyl-3-(3-phenylpropyl)dihydrofuran-2(3H)-one

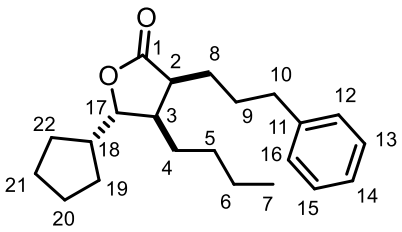

$C_{22}H_{32}O_2$
MW: 329 g.mol^{-1}
Yield: 59% NMR,
12% isolated
d.r.: SM: 6.4 : 1
crude: 69 : 20 : 9 : 2
isolated: 4.5 : 1 : n.d. : n.d.

The compound was obtained following the general procedure B using aldehyde C (19.1 mg, 55 µmol, 1 equiv.) and cyclopentyl magnesium bromide (55 µL of a 2 M Solution in THF, 110 µmol, 2 equiv.) as a colourless oil (2.2 mg, 12 %).

Only major diastereomer characterised.

^{1}H NMR (700 MHz, $CDCl_3$): δ 7.29 – 7.26 (m, 2H, H13+15), 7.20 – 7.17 (m, 3H, H12+14+16), 3.99 – 3.95 (m, 1H, H17), 2.71 – 2.61 (m, 3H, H10+H2), 2.17 – 2.11 (m, 1H, H3), 2.02 (app. dq,

J = 16.6, 8.3 Hz, 1H, H18), 1.84 – 1.64 (m, 8H, H_{aliph}), 1.50 – 1.37 (m, 3H, H_{aliph})), 1.34 – 1.28 (m, 4H, H_{aliph})), 1.23 – 1.14 (m, 3H, H_{aliph})), 0.90 – 0.87 (m, 3H, H7).

^{13}C NMR (176 MHz, $CDCl_3$): δ 178.8 (C1), 141.8 (C11), 128.39 (C_{ar}), 128.36 (C_{ar}), 125.9 (C14), 86.7 (C17), 42.7 (C18), 42.1 (C2), 41.8 (C3), 35.8 (C10), 29.4 (C_{aliph}), 29.2 (C_{aliph}), 29.2 (C_{aliph}), 29.1 (C_{aliph}), 27.0 (C_{aliph}), 25.3 (C_{aliph}), 25.3 (C_{aliph}), 24.6 (C_{aliph}), 22.7 (C_{aliph}), 13.9 (C7).

HRMS (ESI^+): calculated for $C_{18}H_{26}O_2$ $[M+H]^+$ m/z: 329.2475 found $[M+H]^+$ m/z: 329.2472

IR (neat cm^{-1})**:** 2952, 2932, 2862, 1768, 1454, 1185, 745, 700

6. References

(1) Kaur, N.; Grewal, P.; Poonia, K. Dicarbonyl Compounds in O-Heterocycle Synthesis. *Synthetic Communications*. Bellwether Publishing, Ltd. 2021, pp 2423–2444. https://doi.org/10.1080/00397911.2021.1941114.

(2) Brückner, R. *Reaktionsmechanismen*, 3rd edition.; 2004.

(3) Jonathan Clayden, Nick Greeves, S. G. W. *Organic Chemistry*; 2012. https://doi.org/10.1007/s00897010513a.

(4) Mccague, R.; Jarman, M.; Rowlands, M. G.; Mann, J.; Thickitt, C. P.; Clissold, D. W.; Neidle, S.; Webster, G. *Synthesis of the Aromatase Lnhi Bitor 3-Ethyl-3-(4-Pyridyl) Piperidine-2,6-Dione and Its Enantiomers*; 1989.

(5) Bruice, P. Y. *Organic Chemistry, Sixth Edition*; 2011. https://doi.org/10.1016/s0016-0032(26)91405-1.

(6) Omura, S.; Hirano, A.; Iwai, Y.; Masuma, R. HERQULINE, A NEW ALKALOID PRODUCED BY PENICILLIUM HERQUEI FERMENTATION, ISOLATION AND PROPERTIES. *The Journal of Antibiotics* **1979**, 786–790.

(7) Rothenberg, M. L.; Nelson, A. R.; Hande, K. R. New Drugs on the Horizon: Matrix Metalloproteinase Inhibitors. *Stem Cells* **1999**, *17*, 237–240.

(8) Kosuge, T.; Tsuji, K.; Hirai, K. Isolation and Structure Determination of a New Marine Toxin, Neosurugatoxin, From the Japanese Ivory Shell, Babylonia Japonica. *Tetrahedron Letters* **1981**, *22* (35), 3417–3420.

(9) Guo, F.; Clift, M. D.; Thomson, R. J. Oxidative Coupling of Enolates, Enol Silanes, and Enamines: Methods and Natural Product Synthesis. *European Journal of Organic Chemistry*. September 2012, pp 4881–4896. https://doi.org/10.1002/ejoc.201200665.

(10) Baran, P. S.; DeMartino, M. P. Intermolecular Oxidative Enolate Heterocoupling. *Angewandte Chemie - International Edition* **2006**, *45* (42), 7083–7086. https://doi.org/10.1002/anie.200603024.

(11) Jang, H. Y.; Hong, J. B.; MacMillan, D. W. C. Enantioselective Organocatalytic Singly Occupied Molecular Orbital Activation: The Enantioselective α-Enolation of Aldehydes. *J Am Chem Soc* **2007**, *129* (22), 7004–7005. https://doi.org/10.1021/ja0719428.

(12) Stetter, H. *Catalyzed Addition of Aldehydes to Activated Double Bonds-A New Synthetic Approach*; 1976; Vol. 15.

(13) Heravi, M. M.; Zadsirjan, V.; Kafshdarzadeh, K.; Amiri, Z. Recent Advances in Stetter Reaction and Related Chemistry: An Update. *Asian Journal of Organic Chemistry*. Wiley-VCH Verlag December 1, 2020, pp 1999–2034. https://doi.org/10.1002/ajoc.202000378.

(14) Liu, Q.; Rovis, T. Enantio- and Diastereoselective Lntermolecular Stetter Reaction of Glyoxamide and Alkylidene Ketoamides. *Organic Letters* **2009**, *11* (13), 2856–2859. https://doi.org/10.1021/ol901081a.

(15) Kaiser, D.; Teskey, C. J.; Adler, P.; Maulide, N. Chemoselective Intermolecular Cross-Enolate-Type Coupling of Amides. *J Am Chem Soc* **2017**, *139* (45), 16040–16043. https://doi.org/10.1021/jacs.7b08813.

(16) Evano, G.; Coste, A.; Jouvin, K. Ynamides: Versatile Tools in Organic Synthesis. *Angewandte Chemie - International Edition*. Wiley-VCH Verlag April 6, 2010, pp 2840–2859. https://doi.org/10.1002/anie.200905817.

(17) Evano, G.; Blanchard, N.; Compain, G.; Coste, A.; Demmer, C. S.; Gati, W.; Guissart, C.; Heimburger, J.; Henry, N.; Jouvin, K.; Karthikeyan, G.; Laouiti, A.; Lecomte, M.; Martin-Mingot, A.; Métayer, B.; Michelet, B.; Nitelet, A.; Theunissen, C.; Thibaudeau, S.; Wang, J.; Zarca, M.; Zhang, C. A Journey in the Chemistry of Ynamides: From Synthesis to Applications. *Chemistry Letters*. Chemical Society of Japan 2016, pp 574–585. https://doi.org/10.1246/cl.160260.
(18) Dekorver, K. A.; Li, H.; Lohse, A. G.; Hayashi, R.; Lu, Z.; Zhang, Y.; Hsung, R. P. Ynamides: A Modern Functional Group for the New Millennium. *Chemical Reviews* **2010**, *110* (9), 5064–5106. https://doi.org/10.1021/cr100003s.
(19) Dunetz, J. R.; Danheiser, R. L. Copper-Mediated N-Alkynylation of Carbamates, Ureas, and Sulfonamides. A General Method for the Synthesis of Ynamides. *Organic Letters* **2003**, *5* (21), 4011–4014. https://doi.org/10.1021/ol035647d.
(20) Hamada, T.; Ye, X.; Stahl, S. S. Copper-Catalyzed Aerobic Oxidative Amidation of Terminal Alkynes: Efficient Synthesis of Ynamides. *J Am Chem Soc* **2008**, *130* (3), 833–835. https://doi.org/10.1021/ja077406x.
(21) Glaser, C. Beiträge Zur Kenntnis Des Acetenylbenzols. *Berichte der deutschen chemischen Gesellschaft* **1869**, *2* (1), 422–424.
(22) Hay, A. S. Oxidative Coupling of Acetylenes II. *Journal of Organic Chemistry* **1962**, *27*, 3320–3321.
(23) Ghosez, L.; Marchand-Brynaert, J. Cycloadditions of Keteneimmonium Cations to Olefins and Dienes. A New Synthesis of Four-Membered Rings. *J Am Chem Soc* **1972**, *94* (8), 2870–2872.
(24) Madelaine, C.; Valerio, V.; Maulide, N. Revisiting Keteniminium Salts: More than the Nitrogen Analogs of Ketenes. *Chemistry - An Asian Journal*. September 5, 2011, pp 2224–2239. https://doi.org/10.1002/asia.201100108.
(25) Wang, X. N.; Yeom, H. S.; Fang, L. C.; He, S.; Ma, Z. X.; Kedrowski, B. L.; Hsung, R. P. Ynamides in Ring Forming Transformations. *Accounts of Chemical Research* **2014**, *47* (2), 560–578. https://doi.org/10.1021/ar400193g.
(26) Zhang, Y. Syntheses of Vinylindoles via a Brønsted Acid Catalyzed Highly Regio- and Stereoselective Cis-Hydroarylation of Ynamides. *Tetrahedron Letters* **2005**, *46* (38), 6483–6486. https://doi.org/10.1016/j.tetlet.2005.07.098.
(27) Frederick, M. O.; Hsung, R. P.; Lambeth, R. H.; Mulder, J. A.; Tracey, M. R. Highly Stereoselective Saucy-Marbet Rearrangement Using Chiral Ynamides. Synthesis of Highly Substituted Chiral Homoallenyl Alcohols. *Organic Letters* **2003**, *5* (15), 2663–2666. https://doi.org/10.1021/ol030061c.
(28) Mulder, J. A.; Hsung, R. P.; Frederick, M. O.; Tracey, M. R.; Zificsak, C. A. The First Stereoselective Ficini-Claisen Rearrangement Using Chiral Ynamides. *Organic Letters* **2002**, *4* (8), 1383–1386. https://doi.org/10.1021/ol020037j.
(29) Claisen, L. Über Umlagerung von Phenol-Allyläthern InC-Allyl-Phenole. *Berichte der deutschen chemischen Gesellschaft* **1912**, *45* (3), 3157–3166. https://doi.org/10.1002/cber.19120450348.
(30) Castro, A. M. M. Claisen Rearrangement over the Past Nine Decades. *Chemical Reviews* **2004**, *104* (6), 2939–3002. https://doi.org/10.1021/cr020703u.
(31) Bartlett, P. A.; Pizzo, C. F.; Felix, D.; Geschwend-Steen, K.; Wick, A. E.; Eschenmoser, A.; Chim, H.; Mueller, H.; Willard, A. K.; Ficini, J.; Barbera, C.; Lett, T.; Vittorelli, P.; Hansen, H.; Schmid, H.; Negishi, E.; Sabanski, M.; Katz, J.; Brown, H. C.; Jones, T. H.; Blum, M. S.; Fales, M.; Blount, J. F.; Pawson, B. A.; Saucy, G.; Chem Soc, J. D.; Larsen, S. D.; Monti, S. A.; Bartlett, R.; Brockson, T. J.; Li, T.; Faulkner, D. J.; Peterson,

M. R. Evaluation of the Claisen Rearrangement of 2-Cyclohexenols for the Stereoselective Construction of a Terpene Synthon. *Journal of Organic Chemistry* **1981**, *46*, 3896–3900.
(32) Kupczyk-Subotkowska, L.; Saunders, W. H.; Shine, H. J. The Claisen Rearrangement of Allyl Phenyl Ether. *J Am Chem Soc* **1988**, *110*, 7153–7159.
(33) Vance, R.; Rondan, N.; Houk, K. N.; Jensen, F.; Borden, W.; Komornicki, A.; Wimmer, E. Transition Structures for the Claisen Rearrangement. *J Am Chem Soc* **1988**, *110*, 2314–2315.
(34) Arnaud, R.; Dillet, V.; Pelloux-Uon, N.; Annick V, Y. Theoretical Study of the Thio-Claisen Rearrangement. Can Vinylthioethanimine Undergo a [3,3]-Sigmatropic Shift? *Journal of the Chemical Society, Perkin Transactions 2* **1996**, 2065–2071.
(35) Maryasin, B.; Kaldre, D.; Galaverna, R.; Klose, I.; Ruider, S.; Drescher, M.; Kählig, H.; González, L.; Eberlin, M. N.; Jurberg, I. D.; Maulide, N. Unusual Mechanisms in Claisen Rearrangements: An Ionic Fragmentation Leading to a: Meta -Selective Rearrangement. *Chemical Science* **2018**, *9* (17), 4124–4131. https://doi.org/10.1039/c7sc04736c.
(36) Peng, B.; Huang, X.; Xie, L. G.; Maulide, N. A Brønsted Acid Catalyzed Redox Arylation. *Angewandte Chemie - International Edition* **2014**, *53* (33), 8718–8721. https://doi.org/10.1002/anie.201310865.
(37) Kaldre, D.; Maryasin, B.; Kaiser, D.; Gajsek, O.; González, L.; Maulide, N. Asymmetrische Redoxarylierung: Chiralitätstransfer von Schwefel Zu Kohlenstoff Durch Sigmatrope Sulfonium-[3,3]-Umlagerung. *Angewandte Chemie* **2017**, *129* (8), 2248–2252. https://doi.org/10.1002/ange.201610105.
(38) Peng, B.; Geerdink, D.; Farès, C.; Maulide, N. Chemoselective Intermolecular α-Arylation of Amides. *Angewandte Chemie - International Edition* **2014**, *53* (21), 5462–5466. https://doi.org/10.1002/anie.201402229.
(39) Kaldre, D.; Klose, I.; Maulide, N. Stereodivergent Synthesis of 1,4-Dicarbonyls by Traceless Charge-Accelerated Sulfonium Rearrangement. *Science (1979)* **2018**, *361*, 664–667.
(40) Jensen, F. *Introduction to Computational Chemistry*; 2007.
(41) Cramer, C. J. *Essentials of Computational Chemistry Theories and Models Second Edition*; 2004.
(42) Szabo, A.; Ostlund, N. Modern Quantum Chemistry. **1996**.
(43) Koch, W.; Holthausen, M. *A Chemist's Guide to Density Functional Theory*; WILEY-VCH Verlag GmbH: Weinheim, 2002.
(44) Dunning, T. H. Gaussian Basis Sets for Use in Correlated Molecular Calculations. I. The Atoms Boron through Neon and Hydrogen. *The Journal of Chemical Physics* **1989**, *90* (2), 1007–1023. https://doi.org/10.1063/1.456153.
(45) Weigend, F.; Ahlrichs, R. Balanced Basis Sets of Split Valence, Triple Zeta Valence and Quadruple Zeta Valence Quality for H to Rn: Design and Assessment of Accuracy. *Physical Chemistry Chemical Physics* **2005**, *7* (18), 3297–3305. https://doi.org/10.1039/b508541a.
(46) Scuseria, G. E.; Lee, T. J. Comparison of Coupled-Cluster Methods Which Include the Effects of Connected Triple Excitations. *The Journal of Chemical Physics*. 1990, pp 5851–5855. https://doi.org/10.1063/1.459684.
(47) Garcia-Ratés, M.; Becker, U.; Neese, F. Implicit Solvation in Domain Based Pair Natural Orbital Coupled Cluster (DLPNO-CCSD) Theory. *Journal of Computational Chemistry* **2021**, *42* (27), 1959–1973. https://doi.org/10.1002/jcc.26726.

(48) Riplinger, C.; Neese, F. An Efficient and near Linear Scaling Pair Natural Orbital Based Local Coupled Cluster Method. *Journal of Chemical Physics* **2013**, *138* (3). https://doi.org/10.1063/1.4773581.
(49) Hohenberg, P.; Kohn, W. *Inhomogenoeous Electron Gas*; 1964.
(50) Kohn, W.; Sham, L. J. *Self-Consistent Equations Including Exchange and Correlation Effects*; 1965.
(51) Perdew, J. P.; Burke, K.; Ernzerhof, M. *Generalized Gradient Approximation Made Simple*; 1996.
(52) Adamo, C.; Barone, V. Toward Reliable Density Functional Methods without Adjustable Parameters: The PBE0 Model. *Journal of Chemical Physics* **1999**, *110* (13), 6158–6170. https://doi.org/10.1063/1.478522.
(53) Stephens, P. J.; Devlin, F. J.; Chabalowski, C. F.; Frisch, M. J. Ab Initio Calculation of Vibrational Absorption and Circular Dichroism Spectra Using Density Funcional Force Fields. *The Journal of Physical Chemistry* **1994**, *98* (45), 11623–11627.
(54) Lee, C.; Yang, eitao; Parr, R. G. Development of the Colic-Salvetti Correlation-Energy Formula into a Functional of the Electron Density. *Physical Review B* **1988**, *37* (2), 785–789.
(55) Stephens, P. J.; Devlin, F. J.; Ashvar, C. S.; Chabalowski, C. F.; Frisch, M. J. *Theoretical Calculation of Vibrational Circular Dichroism Spectra*; 1994.
(56) Tirado-Rives, J.; Jorgensen, W. L. Performance of B3LYP Density Functional Methods for a Large Set of Organic Molecules. *Journal of Chemical Theory and Computation* **2008**, *4* (2), 297–306. https://doi.org/10.1021/ct700248k.
(57) Andersson, Y.; Langreth, D. C.; Lundqvist, B. I. *Van Der Waals Interactions in Density-Functional Theory*; 1996.
(58) Grimme, S.; Antony, J.; Ehrlich, S.; Krieg, H. A Consistent and Accurate Ab Initio Parametrization of Density Functional Dispersion Correction (DFT-D) for the 94 Elements H-Pu. *Journal of Chemical Physics* **2010**, *132* (15). https://doi.org/10.1063/1.3382344.
(59) Grimme, S.; Ehrlich, S.; Goerigk, L. Effect of the Damping Function in Dispersion Corrected Density Functional Theory. *Journal of Computational Chemistry* **2011**, *32* (7), 1456–1465. https://doi.org/10.1002/jcc.21759.
(60) Zheng, D.; Wang, F. Performing Molecular Dynamics Simulations and Computing Hydration Free Energies on the B3LYP-D3(BJ) Potential Energy Surface with Adaptive Force Matching: A Benchmark Study with Seven Alcohols and One Amine. *ACS Physical Chemistry Au* **2021**, *1* (1), 14–24. https://doi.org/10.1021/acsphyschemau.1c00006.
(61) Smith, D. G. A.; Burns, L. A.; Patkowski, K.; Sherrill, C. D. Revised Damping Parameters for the D3 Dispersion Correction to Density Functional Theory. *Journal of Physical Chemistry Letters* **2016**, *7* (12), 2197–2203. https://doi.org/10.1021/acs.jpclett.6b00780.
(62) van Gunsteren, W.; Oostenbrink, C.; Hansson, T. Molecular Dynamics Simulations. *Current Opinion in Structural Biology* **2002**, *12* (2), 190–196.
(63) Kumar, A.; Baccoli, R.; Fais, A.; Cincotti, A.; Pilia, L.; Gatto, G. Substitution Effects on the Optoelectronic Properties of Coumarin Derivatives. *Applied Sciences (Switzerland)* **2020**, *10* (1). https://doi.org/10.3390/app10010144.
(64) Miertus, S.; Scrocco, E.; Tomasi, J. Electrostatic Interaction of a Solute with a Continuum. A Direct Utilization of Ab Initio Molecular Potentials for the Prevision of Solvent Effects. *Chemical Physics* **1981**, *55*, 117–129.

(65) Barone, V.; Cossi, M. Quantum Calculation of Molecular Energies and Energy Gradients in Solution by a Conductor Solvent Model. *Journal of Physical Chemistry A* **1998**, *102*, 1995–2001.
(66) Takano, Y.; Houk, K. N. Benchmarking the Conductor-like Polarizable Continuum Model (CPCM) for Aqueous Solvation Free Energies of Neutral and Ionic Organic Molecules. *Journal of Chemical Theory and Computation* **2005**, *1* (1), 70–77. https://doi.org/10.1021/ct049977a.
(67) Marenich, A. v.; Cramer, C. J.; Truhlar, D. G. Universal Solvation Model Based on Solute Electron Density and on a Continuum Model of the Solvent Defined by the Bulk Dielectric Constant and Atomic Surface Tensions. *Journal of Physical Chemistry B* **2009**, *113* (18), 6378–6396. https://doi.org/10.1021/jp810292n.
(68) Spicher, S.; Grimme, S. Robust Atomistic Modeling of Materials, Organometallic, and Biochemical Systems. *Angewandte Chemie - International Edition* **2020**, *59* (36), 15665–15673. https://doi.org/10.1002/anie.202004239.
(69) Pracht, P.; Bohle, F.; Grimme, S. Automated Exploration of the Low-Energy Chemical Space with Fast Quantum Chemical Methods. *Physical Chemistry Chemical Physics* **2020**, *22* (14), 7169–7192. https://doi.org/10.1039/c9cp06869d.
(70) Mills, G.; 3onsson, H. *Quantum and Thermal Eff'ects in H2 Dissociative Adsorption: Evaluation of Free Energy Barriers in Multidimensional Quantum Systems*; 1994; Vol. 72.
(71) Mortazavi, B.; Ostadhossein, A.; Rabczuk, T.; van Duin, A. C. T. Mechanical Response of All-MoS2 Single-Layer Heterostructures: A ReaxFF Investigation. *Physical Chemistry Chemical Physics* **2016**, *18* (34), 23695–23701. https://doi.org/10.1039/c6cp03612k.
(72) Henkelman, G.; Uberuaga, B. P.; Jónsson, H. Climbing Image Nudged Elastic Band Method for Finding Saddle Points and Minimum Energy Paths. *Journal of Chemical Physics* **2000**, *113* (22), 9901–9904. https://doi.org/10.1063/1.1329672.
(73) Dennington, R.; Keith, T.; Millam, J. GaussView 6.1.1. Semichem Inc.: Shawnee Mission, KS 2019.
(74) Frisch, M. J.; Trucks, G. W.; Schlegel, H. B.; Scuseria, G. E.; Robb, M. A.; Cheeseman, J. R.; Scalmani, G.; Barone, V.; Petersson, G. A.; Nakatsuji, H.; Li, X.; Caricato, M.; Marenich, A. v.; Bloino, J.; Janesko, B. G.; Gomperts, R.; Mennucci, B.; Hratchian, H. P.; Ortiz, J. v.; Izmaylov, A. F.; Sonnenberg, J. L.; Williams-Young, D.; Ding, F.; Lipparini, F.; Egidi, F.; Goings, J.; Peng, B.; Petrone, A.; Henderson, T.; Ranasinghe, D.; Zakrzewski, V. G.; Gao, J.; Rega, N.; Zheng, G.; Liang, W.; Hada, M.; Ehara, M.; Toyota, K.; Fukuda, R.; Hasegawa, J.; Ishida, M.; Nakajima, T.; Honda, Y.; Kitao, O.; Nakai, H.; Vreven, T.; Throssell, K.; Montgomery, J. A. Jr.; Peralta, J. E.; Ogliaro, F.; Bearpark, M. J.; Heyd, J. J.; Brothers, E. N.; Kudin, K. N.; Staroverov, V. N.; Keith, T. A.; Kobayashi, R.; Normand, J.; Raghavachari, K.; Rendell, A. P.; Burant, J. C. ; Iyengar, S. S.; Tomasi, J.; Cossi, M.; Millam, J. M.; Klene, M.; Adamo, C.; Cammi, R.; Ochterski, J. W.; Martin, R. L.; Morokuma, K.; Farkas, O.; Foresman, J. B.; Fox, D. J. Gaussian 16. Gaussian Inc.: Wallingford CT 2016.
(75) Neese, F. The ORCA Program System. *Wiley Interdisciplinary Reviews: Computational Molecular Science* **2012**, *2* (1), 73–78. https://doi.org/10.1002/wcms.81.
(76) Neese, F. Software Update: The ORCA Program System, Version 4.0. *Wiley Interdisciplinary Reviews: Computational Molecular Science* **2018**, *8* (1). https://doi.org/10.1002/wcms.1327.

(77) TURBOMOLE V7.2 a Development of University of Karlsruhe and Forschungszentrum Karlsruhe GmbH, 1989-2007, TURBOMOLE GmbH, since 2007. 2017.